Review | Received 17 March 2026; Revised 28 May 2026; Accepted 4 June 2026; Published XX June 2026
https://doi.org/10.55092/aimat20260007

Optimization of assembly for enhancing light collection efficiency in scintillation detectors

Yuze Hua, Xuxin Yang, Jinzhu Chen, Xuesong Li* and Yang Liu*

North China Electric Power University, School of Nuclear Science and Engineering, Beijing 102206, China

* Correspondence authors; E-mails: lxs@ncepu.edu.cn (X.L.); yliu@ncepu.edu.cn (Y.L.).

Highlights:

- System-level assembly strategies for improving scintillator light collection efficiency.
- Couples geometry, surface finish, reflectors and optical coupling to reduce losses.
- Matching between scintillators and photodetectors for efficient signal readout.
- AI-assisted design strategies provide new opportunities for scintillator assembly optimization.

Abstract: As a core technology for ionizing radiation detection, the performance of scintillation detectors has improved significantly over the past few decades, and their key components, such as scintillators and photodetectors, have also undergone multiple iterations. However, little attention has been paid to the fact that, besides the intrinsic properties of materials and the quantum efficiency of photodetectors, the assembly matching between components also plays a decisive role in the overall performance of the detector, as reflected in improved light collection efficiency (LCE). Therefore, a systematic investigation into the influence of assembly optimization on LCE is of great significance for promoting the development of high-performance scintillation detectors. This paper first defines the concept of LCE and clarifies its influence on the key performance of scintillation detectors. Subsequently, focusing on assembly optimization, it outlines improvements in LCE through multi-interface optical synergy among scintillators, reflective layers and coupling media. Finally, the effective conversion of collected photons into measurable electrical signals is promoted through rational photodetector matching, thereby further improving the overall detection efficiency of scintillation detection systems. In addition, the emerging role of AI-assisted design in scintillation-detector assembly optimization is discussed as a forward-looking perspective. This review systematically summarizes and compares LCE-enhancement strategies at the assembly level, extracts transferable design guidelines from different optimization approaches, and outlines a possible future workflow for AI-assisted assembly optimization.

Keywords: scintillation detector; light collection efficiency (LCE); assembly optimization; optical coupling; photodetector selection; AI-assisted design

1. Introduction

As an important technology for ionizing radiation detection, the optimization of scintillation detector performance has been a central research topic in relevant fields since their inception. Numerous studies have focused on improving the luminescence efficiency of scintillators, developing novel scintillation materials, and enhancing the quantum efficiency and response characteristics of photodetectors [1–5]. These advances have significantly promoted the applications of scintillation detectors in nuclear radiation detection, medical imaging, homeland security, industrial non-destructive testing, and other fields [6–9]. However, in addition to the intrinsic properties of materials and photodetectors, the inter-component assembly configuration also decisively influences the overall performance of scintillation detectors [10–11].

During the process from photon generation in the scintillator to conversion into electrical signals by the photodetector, photons undergo a series of propagations and cross-interface transmissions, resulting in considerable photon loss. Scintillator materials generally have a high refractive index, which differs significantly from that of the surrounding medium (primarily air, with a refractive index of 1), making total internal reflection highly likely at the interface [12]. Owing to the intrinsic absorption of scintillators, the longer photon propagation path within the scintillator further increases the probability of photon absorption, resulting in greater photon loss [13]. Even photons successfully exiting the scintillator may fail to be collected by the effective sensitive area of the photodetector due to mismatched interfacial optical properties or an exit angle distribution that deviates from the optimal incidence conditions [14]. In addition, the main emission band of scintillators must match the high-response region of photodetectors to achieve efficient signal conversion [15,16]. These multiple loss mechanisms collectively reduce light collection efficiency (LCE).

To improve LCE, researchers have proposed a variety of technical strategies. For instance, photonic crystals can be introduced onto the scintillator surface to enhance the probability of photon escape by regulating the local density of electromagnetic states and the exit angle distribution [12,17]; optimizing the geometric design of the scintillator can alter the photon propagation path and exit angle distribution, thereby reducing the probability of internal total internal reflection [18,19]. In addition, common strategies include depositing reflective layers with high reflectivity on the scintillator surface and employing refractive-index-matched optical coupling agents between the scintillator and photodetectors, all of which have achieved favorable results [11,20]. However, the conversion process from optical to electrical signals involves multiple components, such as scintillators, reflective layers, coupling media, and photodetectors, and the level of LCE depends on the synergistic interactions among these components. To date, there is still a lack of comprehensive review studies on LCE optimization achieved through improved assembly configurations of these components.

Based on the above discussion, this review summarizes assembly-level strategies for improving the LCE of scintillation detectors from the perspective of the optical transport chain. By comparing their mechanisms, applicable conditions, and limitations, this review aims to provide practical design guidance for high-performance scintillation detectors. Firstly, the working principle of scintillation detectors and the physical connotation of LCE are summarized, and its key role in energy resolution and the signal output chain is clarified. Subsequently, the discussion is carried out from the two aspects of photon generation and transport: on the one hand, the focus is placed on the selection of scintillator materials and the optimization of their geometric structure and surface treatment; on the other hand, the

rational configuration principles of light collection subsystems such as reflective layers, optical coupling media, and light guide structures are summarized. Finally, combined with the emission spectrum of scintillators and application requirements, the selection and matching strategies of photodetectors are discussed to maximize the conversion probability of photons arriving at the sensitive area into photoelectrons, thereby improving the overall detection efficiency of the system. In addition to summarizing conventional assembly strategies, this review further discusses the emerging role of artificial intelligence in accelerating detector design. In particular, AI-assisted surrogate modeling, inverse design, and multi-objective optimization are highlighted as promising tools for navigating the highly coupled parameter space of scintillation detector assembly.

2. Principles and light collection efficiency of scintillation detectors

A scintillation detector is a type of radiation detection device that converts the energy of incident ionizing radiation into an optical signal, which is further converted into an electrical signal for output. Its basic configuration generally consists of a scintillator, a photodetector, a light-collection and optical-coupling system, and subsequent signal-processing electronics [21]. Its working principle is illustrated in Figure 1.

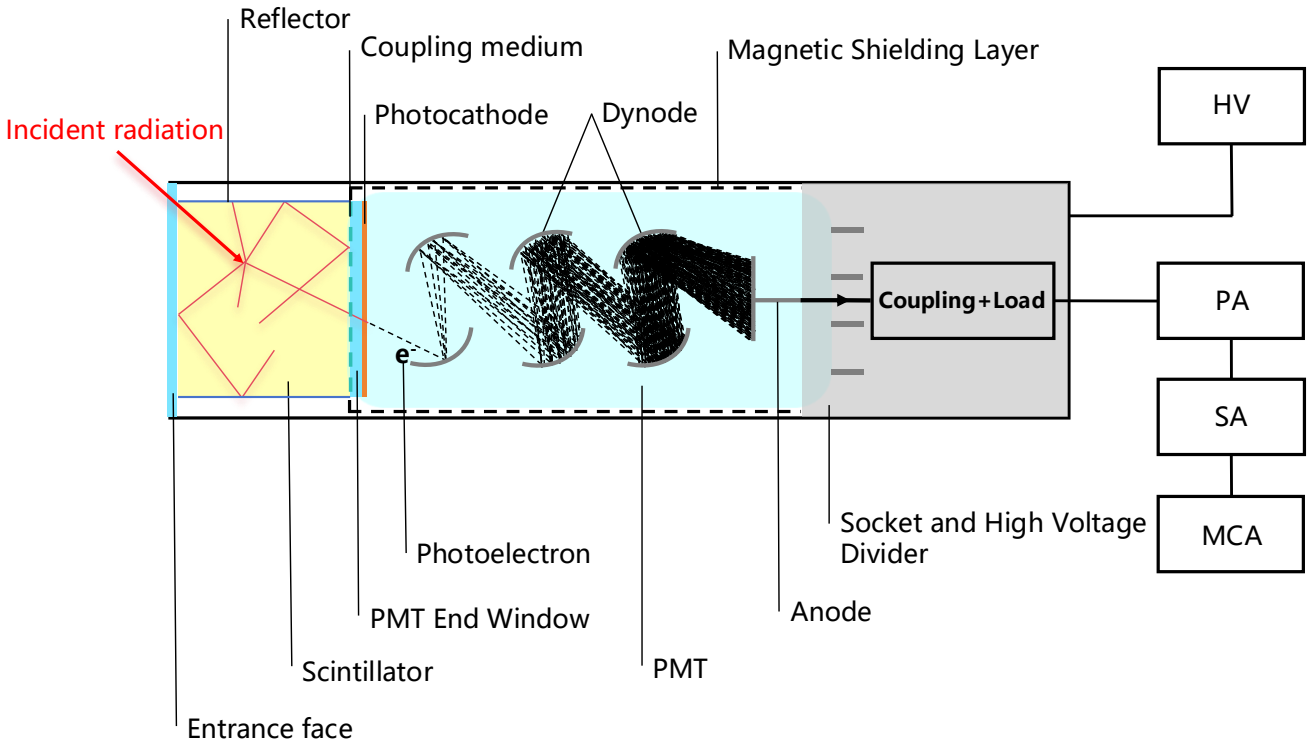

Figure 1. Working principle of typical scintillation detectors.

During the process from photon generation to reception by the detector, photons undergo complex physical losses (e.g., crystal self-absorption, losses from surface reflection, and trapping caused by total internal reflection at interfaces), which result in only a fraction of photons being able to successfully escape from the crystal and reach the detector. To quantitatively describe the effectiveness of this optical transport process, the concept of LCE has been introduced in the academic field to characterize the proportion of photons that can overcome transport losses and finally arrive at the sensitive area of the

photodetector among the total number of photons generated inside the scintillator [22]. Its mathematical expression is generally defined as follows:

$$[\mathrm{LCE} = \frac{\mathrm{N_{arrival}}}{\mathrm{N_{generated}}}] \quad (1)$$

$N_{generated}$ is the total number of photons excited by incident particles in the scintillator (depending on the light yield of the material), and $N_{arrival}$ is the number of photons that actually reach the sensitive surface of the photodetector after optical transport. LCE describes the geometric and optical transport efficiency of photons, excluding the photoelectric conversion process. The final performance of the detector also needs to consider the ability of the photodetector to convert collected photons into photoelectrons, namely:

$$[N_{pe} = N_{generated} \times LCE \times \varepsilon] \quad (2)$$

In Equation (2), N_{pe} denotes the number of effective photoelectrons, and ε represents the combined factor of the effective quantum efficiency (QE_{eff}) and the photoelectron collection efficiency (CE). According to Poisson statistics, when the detection process is limited by statistical fluctuations, the energy resolution is inversely proportional to the square root of the number of photoelectrons ($R \propto 1 / \sqrt{N_{pe}}$). Therefore, under the premise that the detector quantum efficiency (QE) is fixed, maximizing LCE is one of the most direct and critical approaches to improve the energy resolution of the detector, reduce statistical noise, and enhance the signal-to-noise ratio (SNR) [23].

Based on the above link decomposition, improving the performance of scintillation detectors can be attributed to the synergistic optimization of loss mechanisms across the three stages of luminescence, transport, and photoelectric conversion [24]. This paper focuses on assembly optimization to improve LCE. At the scintillator level, LCE is mainly restricted by the photon transport characteristics inside the crystal. Scattering and self-absorption of photons inside the scintillator are the dominant loss sources. The total internal reflection mode can be effectively disrupted, and the photon escape probability can be increased through crystal shape design and surface microstructure modulation [25]. At the optical transport and coupling interface, losses primarily result from boundary escape and refractive-index mismatch. To this end, the crystal side surfaces are often coated with reflective layers that provide diffuse or specular reflection to achieve directional photon convergence, and optical coupling media are used to establish a transition channel with a refractive index gradient, thereby minimizing Fresnel reflection loss at the interface. From this perspective, LCE is jointly governed by geometry, interface conditions, and detector response, and can therefore serve as a physically meaningful target metric for subsequent data-driven modeling, surrogate learning, and multi-objective optimization. In addition to these methods for directly improving LCE, the exploitation of terminal detection performance is equally important. Appropriate photodetector selection and matching ensure that photons reaching the readout end are efficiently converted into measurable electrical signals [26,27].

3. Selection and optimization of scintillators

As the signal source in the detection chain, the effective light output of a scintillator is jointly determined by its intrinsic light yield and light extraction efficiency. The essence of scintillation detection lies in the energy deposition and conversion processes triggered by the interaction of high-energy radiation with

matter. When high-energy particles or rays are incident on the scintillation medium, they deposit energy in the material through ionization and excitation, generating excited species or carriers and enabling energy transfer; subsequently, the excited luminescent molecules or luminescent centers undergo de-excitation via radiative relaxation, releasing part of the deposited energy in the form of scintillation photons [15]. Figure 2 illustrates the microscopic luminescence process in inorganic scintillators, including energy deposition, carrier relaxation, and photon emission. This intrinsic luminescence property establishes scintillators' central role as photon emitters in the signal generation stage. However, the intensity of the final detection signal depends not only on the initial light yield but also on the photon transport and extraction processes inside the scintillator.

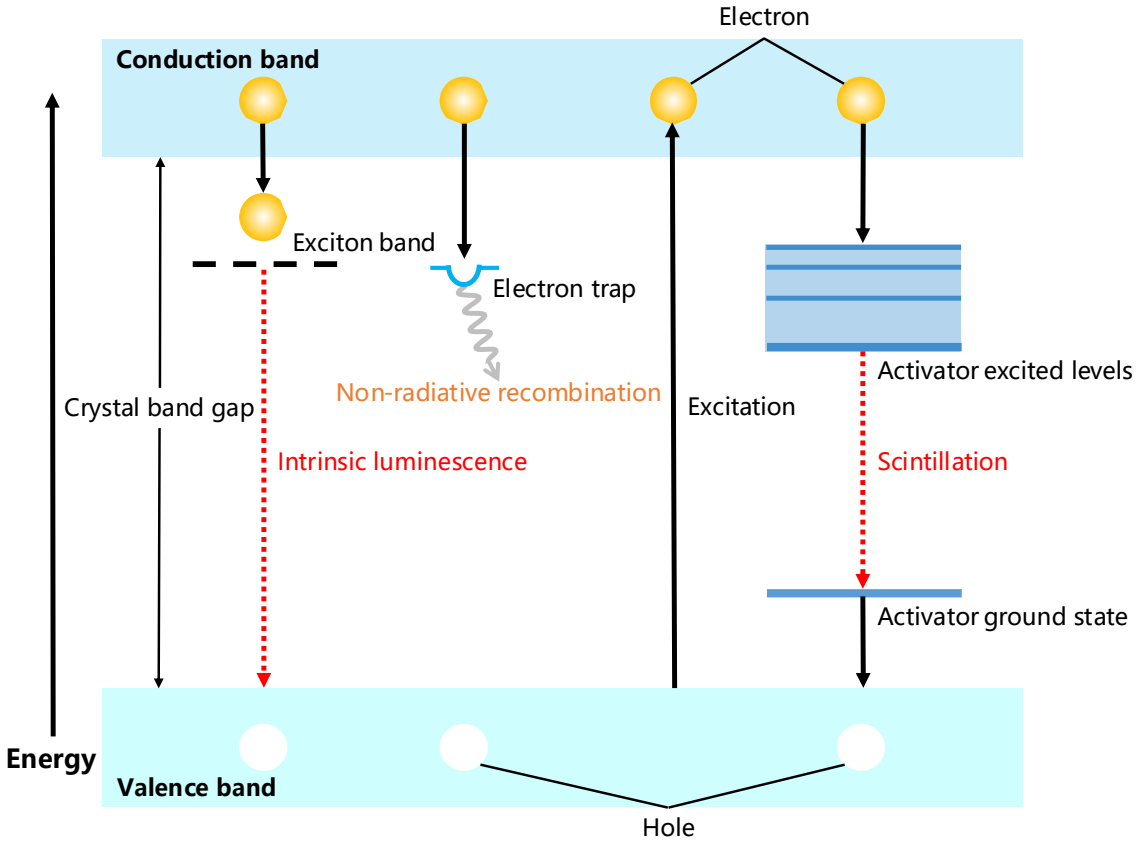

Figure 2. Microscopic energy conversion and photon generation mechanism induced by high-energy particles incident on inorganic crystals.

Specifically, the intrinsic light yield determines the theoretical upper limit of the detection system's signal output, while the light extraction efficiency is primarily limited by processes such as crystal self-absorption and interfacial total internal reflection (TIR). The refractive index of most scintillators is approximately 1.5–2.2, which is significantly different from that of the external medium (usually air, $n \approx 1.0$), resulting in a small critical angle. Some photons are trapped inside the crystal due to satisfying the total internal reflection condition (Figure 3), which prolongs the photon propagation path and accumulates absorption and scattering losses, ultimately reducing the number of effective photons reaching the photodetector. On this basis, this section is organized into two aspects: "signal generation" and "photon transport". Firstly, the selection of scintillators is discussed based on radiation type and detection requirements to ensure a sufficient initial photon yield. Subsequently, focusing on engineering

optimization, it is clarified that the photon trajectory is regulated through geometrical design and surface treatment to weaken the total internal reflection-related trapping and reduce internal losses, thereby improving the photon escape probability and the overall collection efficiency.

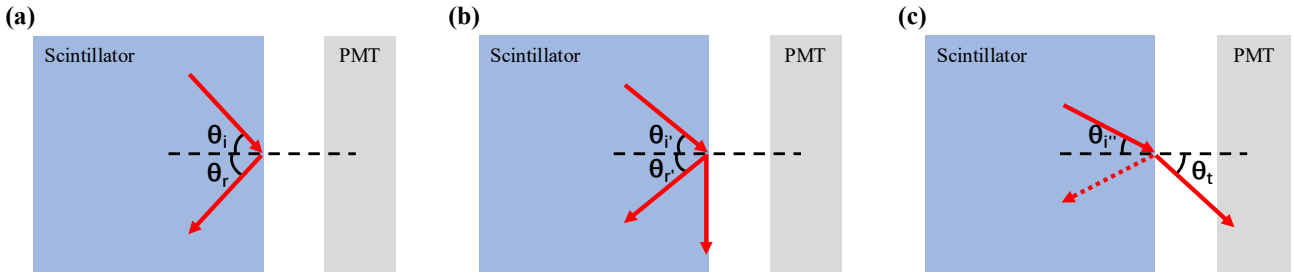

Figure 3. Schematic diagram of the TIR critical angle and photon escape cone at the scintillator exit interface. The refractive index of air is n_1, and the refractive index of the scintillator is n_2, where $\sin\theta_c = n_1 / n_2$: **(a)** $\theta_i > \theta_c$; **(b)** $\theta_{i'} = \theta_c$; **(c)** $\theta_{i''} < \theta_c$.

3.1. Selection of scintillators

When selecting scintillators, it is necessary to first clarify the type and energy range of the radiation to be detected, since different ionizing radiations exhibit distinct energy deposition behaviors in materials [15]. For instance, inorganic scintillators with high effective atomic number and high density are preferred for X-ray and gamma-ray detection [21]. Alpha particles feature short range and prominent surface energy deposition, so thin-layer, coated or flake scintillators are commonly adopted [28–30]. For beta particle detection, scintillator thickness is determined according to particle energy and detection efficiency, and organic or plastic scintillators with low effective atomic numbers help suppress bremsstrahlung interference [31]. For neutron detection, thermal neutrons usually require ^{6}Li, ^{1}B and Gd conversion components, while fast neutrons are commonly detected using hydrogen-rich organic liquid or plastic scintillators [32–34].

After this initial screening, scintillators should be further selected according to application-specific requirements such as light yield, density, decay time, energy resolution, radiation tolerance, chemical stability, and cost. For example, NaI: Tl is suitable for conventional gamma-ray spectroscopy because of its high light yield and mature technology [35]; LYSO: Ce is widely used in PET owing to its high density and fast decay [36]; and $LaBr_3$: Ce combines high light yield, rapid decay and superior energy resolution, making it applicable to high-resolution gamma spectroscopy and miniaturized detection systems [37]. More detailed discussions of scintillator materials and applications can be found in the reviews by Dujardin *et al.* [9] and Lecoq *et al.* [38].

3.2. Optimization of scintillators

3.2.1. Geometrical structure

Changing the scintillator's geometrical shape essentially controls the distribution of photon transport within the medium. The total light yield is determined by the material's intrinsic properties, while the number of collectible photons depends on the balance between transmission efficiency and loss mechanisms. Due to the bulk absorption and surface scattering in crystals, the longer the optical path of

photons inside the scintillator and the greater the number of reflections, the higher the probability of photon attenuation [39,40]. Therefore, the core of geometrical optimization lies in breaking photon-trapping paths caused by total internal reflection and shortening the average optical path for photons to reach the detection end [41].

The scintillator volume and aspect ratio jointly determine the balance between radiation stopping efficiency and effective light output [18,42]. Increasing the volume can improve radiation absorption, but it also increases the average optical path and may enhance bulk absorption losses [15,43,44]. For example, Sasano *et al.* showed that the light output of BGO crystals generally decreases with increasing crystal size under the same APD readout and reflective-coating conditions, and deeper crystals tend to exhibit lower light collection efficiency for the same readout area [40]. Similarly, Pauwels *et al.* [45] observed that slender LSO: Ce crystal strips with higher aspect ratios produced lower light output than shorter and thicker crystals.

Breaking the geometrical symmetry of scintillators is an effective strategy for improving light output, because it can disrupt cyclic reflection paths and modify the exit-angle distribution of photons [42,46]. Tapered structures, such as conical scintillators, can act as optical funnels and reduce repeated internal reflections in regular crystals [18,47]. For example, Sosa *et al.* [48] showed that, compared with cylindrical trans-stilbene, a tapered geometry significantly reduced the average number of internal reflections, thereby improving light collection efficiency and energy resolution (Figure 4a). Their subsequent work further demonstrated that this optimization also enhanced neutron–gamma pulse shape discrimination, especially in the low-light-output region [49]. In addition to tapered geometries, non-conventional prismatic structures can also improve light collection behavior. Studies on $CaWO_4$ crystals showed that, at similar volumes, hexagonal prisms exhibited higher light collection efficiency than cylindrical and rectangular geometries, while triangular prisms achieved the highest light output and better energy resolution (Figure 4b) [18]. These results indicate that non-axisymmetric or tapered geometries can improve LCE by regulating photon reflection paths and exit-angle distributions, without substantially increasing the scintillator volume [50].

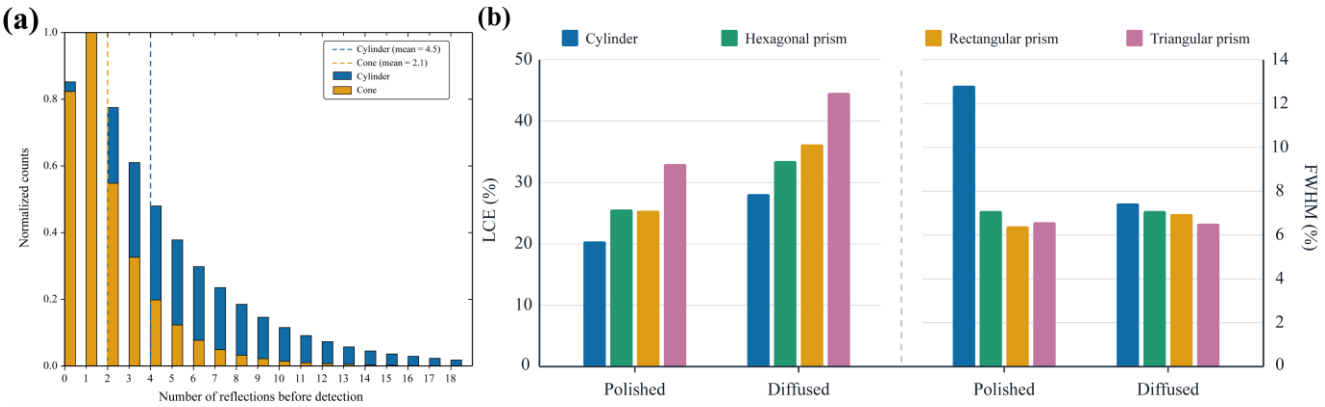

Figure 4. Geometrical structure optimization of scintillators: **(a)** Comparison of the average number of optical-photon reflections before detection in cylindrical and conical trans-stilbene scintillators [48]; **(b)** Comparison of LCE and FWHM for scintillators with different geometries and surface treatments [18]. Redrawn by the authors based on the data and concepts reported in [18,48].

3.2.2. Surface treatment

Grinding and polishing are the main techniques for regulating the surface optical properties of scintillators (Figure 5a). By modifying microscopic roughness, they produce interfaces dominated by either specular or diffuse reflection [51]. A polished surface tends to preserve photon directionality and supports total-internal-reflection-based light guiding, whereas a roughened surface randomizes photon directions and approximately follows Lambertian scattering behavior [51,52].

The optimal surface treatment depends strongly on scintillator geometry. For low-aspect-ratio crystals, such as bulk or cubic scintillators, photon trapping caused by repeated total internal reflection is often a major source of light loss [18]. In this case, roughened or etched surfaces can disrupt stable reflection loops, redistribute photon directions, and increase the probability of photons entering the escape cone, thereby improving light collection efficiency [18,53–56]. In contrast, for slender strip- or fiber-like scintillators, photon transport is dominated by long-distance guiding along the crystal axis. Polished surfaces are therefore preferred because they preserve specular propagation and reduce scattering-induced path-length broadening, whereas diffuse scattering may increase the average optical path and aggravate bulk absorption [19,57–59]. The dependence of light output and photon-arrival-time spread on crystal length under grinding and polishing treatments is shown in Figure 5b,c.

Surface treatment also involves a trade-off between energy and timing performance [11,60]. Roughened surfaces or diffuse reflection can increase light output and may improve energy resolution, but they also broaden the photon arrival-time distribution due to increased optical-path uncertainty [61,62]. Conversely, polished surfaces help retain direct or early-arriving photons and reduce transit-time jitter, which is particularly important for timing-sensitive applications such as TOF-PET [63,64].

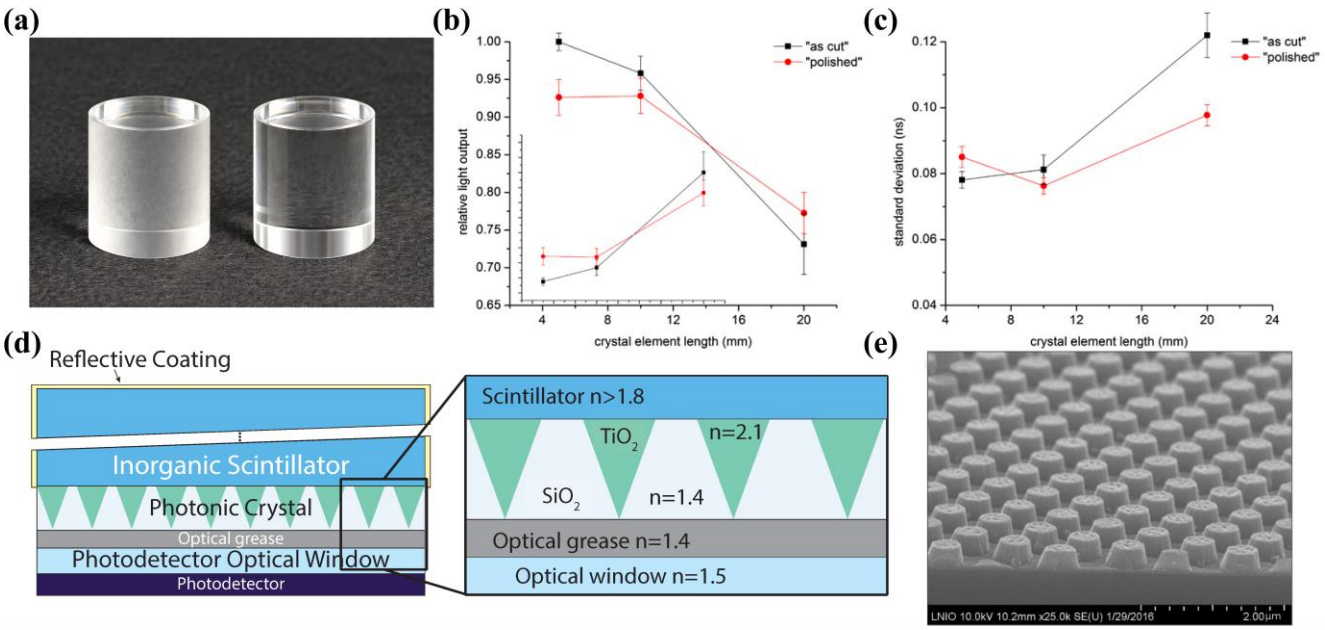

Figure 5. Surface treatment of scintillators: **(a)** Grinding and polishing treatments; **(b)** Variation of light output with crystal length [58]; **(c)** Variation of standard deviation of arrival time with crystal length [58]; **(d)** Photonic crystal applied to the output end face of the scintillator in scintillation detectors [61]; **(e)** SEM image of TiO_2 photonic crystal pattern [65]. Reprinted with permission from [58,61,65]. Copyright 2011 IOP Publishing.

Beyond conventional grinding and polishing, photonic crystal structures have been introduced to improve light extraction at scintillator surfaces (Figure 5d) [61]. These subwavelength periodic structures, such as holes, pillars, cones, or pyramids, provide diffraction channels and act as effective refractive-index transition layers, thereby reducing total-internal-reflection limitations caused by refractive-index mismatch (Figure 5e) [65,66]. As a result, they can enhance light extraction while reducing photon trapping and bulk absorption losses [67].

4. Optimization of the light collection system

Previous sections have discussed improving the light generation and extraction efficiency inside scintillators through material selection, surface treatment, and geometrical optimization. This section shifts the focus to the external light-collection system, emphasizing the optimization of components, including reflective layers, optical coupling agents, and light guides [15]. The content covers type selection and spectral matching of reflective layers, the refractive-index-coupling mechanism at the scintillator-detector interface, and the role of light guides in geometric regulation and uniformity improvement. Through collaborative optimization of the external optical link, the aim is to minimize transmission loss and approach the theoretical upper limit of the detector's light-collection efficiency.

4.1. Reflective layers

4.1.1. Types of reflective layers

To prevent lateral photon leakage and improve light output, scintillator surfaces are commonly wrapped or coated with reflective layers [14]. According to their reflection mechanisms, commonly used reflectors can be classified into specular materials, such as aluminum, silver, and Enhanced Specular Reflector (ESR), and diffuse materials, such as PTFE and TiO_2 powder (Figure 6a). The effectiveness of a reflector depends strongly on its compatibility with the scintillator surface treatment, because different combinations of specular and diffuse reflection regulate photon recycling and angular redistribution at the interface (Figure 6b) [68,69].

For high-aspect-ratio scintillators or systems requiring long-distance light guiding, polished side walls combined with specular reflectors are generally preferred. In this configuration, photon transport is mainly maintained by total internal reflection, while photons escaping due to unsatisfied total internal reflection conditions or non-ideal interfaces can be redirected by the external specular reflector [64,70–72]. Compared with diffuse reflection, specular reflection better preserves photon directionality and suppresses angular broadening, thereby reducing arrival-time dispersion in timing-sensitive applications [60,63,65,73].

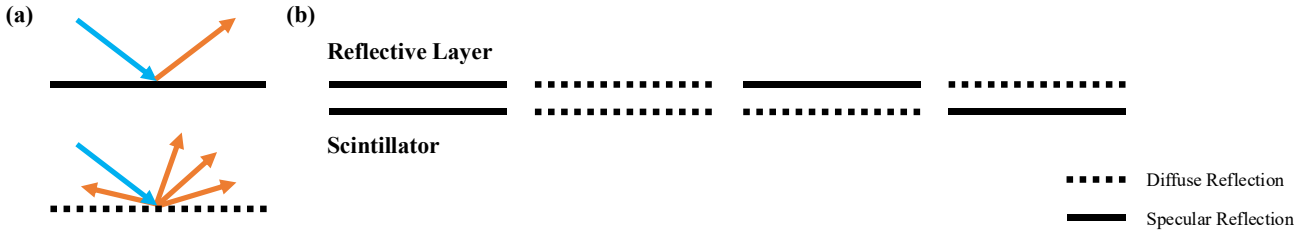

Figure 6. Surface reflection types of scintillators.

For low-aspect-ratio scintillators, such as bulk, flat, or nearly cubic crystals, roughened side walls combined with diffuse reflectors often provide higher LCE when the main goal is to enhance light output and energy resolution [58,74]. Rough surfaces disrupt stable total-internal-reflection trapping paths, while near-Lambertian diffuse reflectors such as PTFE and TiO_2 recycle laterally escaping photons by randomizing their directions, increasing the probability that photons enter the escape cone at the readout end [58,74–76]. Although this strategy may increase the average optical path and broaden the photon arrival-time distribution, the gain from reduced trapping can be dominant when self-absorption is not severe [58,73,74].

A compromise scheme combining polished surfaces with diffuse reflective coating is often adopted in practical detector assemblies, particularly for hygroscopic scintillators requiring encapsulation or large-volume bulk crystals [77]. In this configuration, photons are first transported along the polished interface through total internal reflection, while those escaping because the TIR condition is not satisfied pass through the interfacial gap and are scattered back by the external diffuse reflector [77,78]. This multistage reflection process balances transmission stability and light-output enhancement [61,77].

4.1.2. Selection of reflective layer materials

The primary step in material selection is to identify the scintillator's emission wavelength band, and priority should be given to materials with high reflectivity in this band [11]. Since reflectivity shows a strong wavelength dependence (Figure 7), band mismatch can significantly reduce the reflection gain. Relevant reflectivity data can be obtained from the systematic study by Martin Janecek on the spectral reflection characteristics of reflective materials [14,76]. The operating wavelength ranges of common reflective layer materials are listed in Table 1.

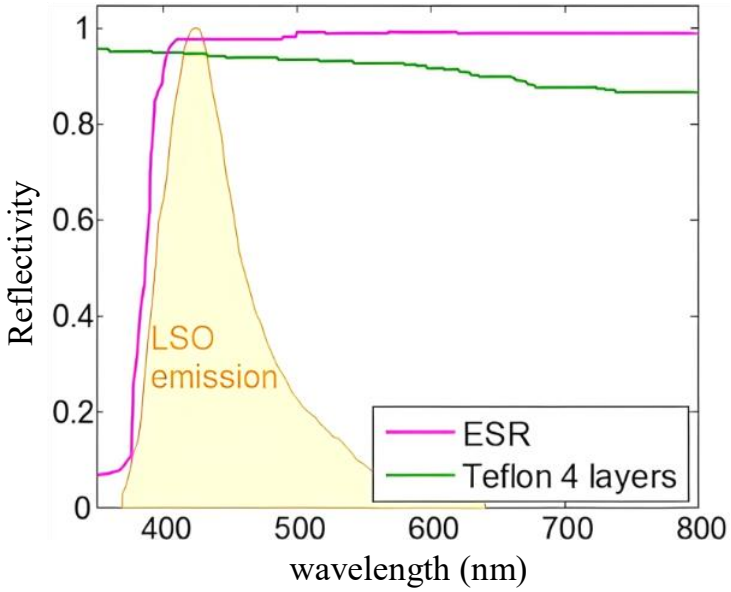

Figure 7. Reflectivity spectral characteristics of different reflective materials [19]. Reprinted with permission from [19]. Copyright 2017 IOP Publishing.

Table 1. Representative reflector materials for scintillation detectors and their typical spectral applicability.

Material	Reflection	Type	Typical Applicable Wavelength Range (nm)
Al	Specular reflection	Metallic coating	200–2000 [79]
Ag	Specular reflection	Metallic coating	450–2000 [79]
Au	Specular reflection	Metallic coating	700–2000 [79]
PTFE	Diffuse reflection	Polymer	400–1500 [80]
Tyvek	Diffuse reflection	Polymer	400–700 [81]
$BaSO_4$	Diffuse reflection	Inorganic powder/coating	200–2000 [82]
TiO_2	Diffuse reflection	Inorganic powder/coating	400–700 [83]
MgO	Diffuse reflection	Inorganic powder/ceramic	400–700 [84]
Aluminum foil	semi-diffuse reflection	Metal rolled foil	250–2500 [85]
ESR	Specular reflection	Multilayer polymer	400–800 [86]
Melinex/Lumirror	Diffuse reflection	Polyester film	400–700 [87]

In addition to spectral matching, the crystal geometry and array packing density also determine the morphology of the reflective layer material [88]. In high-spatial-resolution PET arrays, the gap between crystals is extremely small, making it difficult to use thick diffuse reflection materials. In this case, ESR film with a thickness of approximately 65 μm and good mechanical stiffness can maintain a high packing factor while preserving high light transmission efficiency [88–91]. For complex surfaces such as spherical, hemispherical, or shaped light guides, sheet materials are difficult to conform seamlessly. Diffuse reflection coatings based on TiO_2 or $BaSO_4$ are more suitable due to their strong adhesion and flexible processing, but multilayer spraying is required to reduce the risk of cracking during curing [92].

Chemical stability and hygroscopicity of materials also constitute important engineering constraints [93]. For highly hygroscopic halide scintillators (e.g., NaI: Tl, $LaBr_3$), PTFE exhibits high chemical inertness, but its porous structure makes it difficult to block water vapor. Therefore, it is usually only used as an inner reflective medium and must be combined with aluminum or stainless steel housings to achieve hermetic packaging [93]. On the other hand, in TOF-PET, aiming for picosecond-level time resolution, specular reflection materials are often selected at the expense of partial light yield to preserve the directionality of Cherenkov light and reduce time broadening caused by optical path differences, thereby achieving faster transient response [94–96].

4.1.3. Thickness consideration of reflective layer materials

In the optical model of scintillation detectors, the reflective layer thickness is not only a geometric parameter but also affects the photon escape probability and light collection efficiency [19].

The high reflectivity of diffuse reflection materials arises from multiple bulk scatterings induced by their microstructure, making them highly sensitive to thickness when used as reflective layers [76]. Such materials are generally translucent, and photons must penetrate to a certain depth to be efficiently backscattered. When the thickness is below the threshold, insufficient optical density leads to photon transmission through the layer or absorption by the housing. Roncali *et al.* [19] pointed out that within this thin-layer regime, each additional layer of the reflective material results in an approximately linear and significant increase in light collection efficiency (Figure 8a). As thickness increases, transmission is gradually suppressed, and reflectance approaches a limiting value (> 98%) once the saturation thickness is reached; further thickening yields negligible gain in LCE (Figure 8b) [97,98]. Therefore, large-volume single-crystal detectors should ensure that the diffuse reflection layer thickness lies in the saturation region with sufficient margin to avoid transmission leakage.

Unlike diffuse reflection materials, specular reflection materials reflect photons relying on surface coatings or optical interference structures [99]. They are inherently opaque, and their thickness has negligible influence on reflectivity (e.g., a 0.065 mm-thick ESR film already exhibits reflectivity above 98% [100]). Excessively thick reflective layers will reduce the detector's geometric packing factor and degrade mechanical conformability [90]. Therefore, under the premise of satisfying opacity, the key engineering selection criterion for such materials is to ensure complete coverage and mechanical strength of the film, rather than blindly increasing thickness.

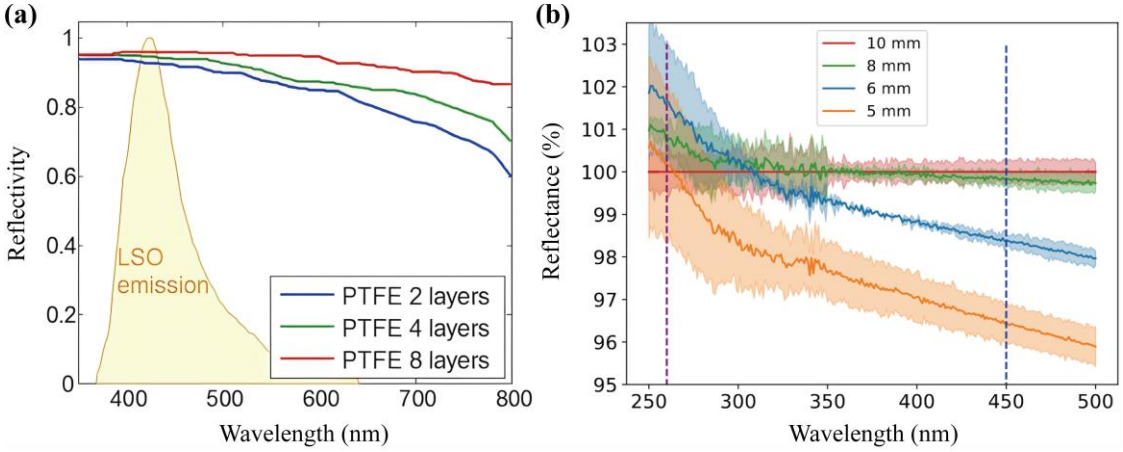

Figure 8. Variation of PTFE reflectivity with thickness [19,98]. Reprinted with permission from [19,98]. Copyright 2017, 2020 IOP publishing.

4.2. Coupling agents and light guides

4.2.1. Selection of coupling media

Optical coupling media are critical materials for reducing interfacial losses among scintillators, light guides, and photodetector windows. Their primary function is to fill microscopic air gaps between adjacent optical components and to establish a smoother refractive-index transition, thereby reducing Fresnel reflection and total internal reflection losses. Makek *et al.* [101] reported that, in a Lutetium Fine Silicate (LFS) scintillator matrix coupled to a SiPM array, the use of BC-630 silicone optical grease increased the signal amplitude by up to approximately 40% and also improved the energy resolution.

The selection of coupling media should comprehensively consider refractive index, spectral transmittance, assembly mode, and long-term stability. In general, the refractive index of the coupling material should lie between those of the scintillator and the photodetector entrance window or light guide, and the material should maintain high transmittance over the scintillator emission band. Taking EJ-550 silicone grease as an example, its refractive index is approximately 1.46. At a thickness of 0.1 mm, its transmittance is higher than 90% in the 300–500 nm range, whereas it decreases markedly when the wavelength is below 300 nm [102].

For applications requiring temporary coupling or convenient replacement, silicone grease is generally more suitable, whereas optical adhesives, optical cements, or optical interface pads may be selected for long-term fixed connections depending on the specific interface. Meanwhile, the long-term stability of the coupling material is also important, since temperature variation, irradiation, yellowing, evaporation, bleeding, or interfacial delamination may degrade optical transmission. Romanchek *et al.* [103]

performed 2 h temperature-exposure tests on several coupling materials from −20 to 50 °C. The results showed that the energy resolution at 662 keV varied with both the coupling material and the thermal history, with values ranging from 9.8% to 13.3% for BC-630 and from 10.2% to 14.6% for OG0010. Therefore, the selection of coupling media should not rely solely on refractive index and initial transmittance, but should also account for the actual operating temperature, interface structure, and long-term stability.

4.2.2. Design of light guides

In the light-collection chain of scintillation detectors, light guides do not increase the intrinsic light yield but convert the direct coupling between the scintillator and the photodetector into a designable optical channel to maximize the retention of readable photons under engineering constraints [15]. They are mainly used to alleviate four types of coupling issues: achieving aperture and shape transition through a tapered cross-section to reduce geometric mismatch and response non-uniformity (Figure 9a) [104–106]; extracting optical signals from strong magnetic fields, high temperatures, or high-radiation environments to protect sensitive devices and front-end electronics (Figure 9b) [107,108]; enabling flexible layout and improved integration via bent optical paths in space-constrained systems [105,109]; and implementing optical signal mapping and multiplexing from multiple pixels to fewer channels using a light-guide matrix in array readout (Figure 9c) [109–111].

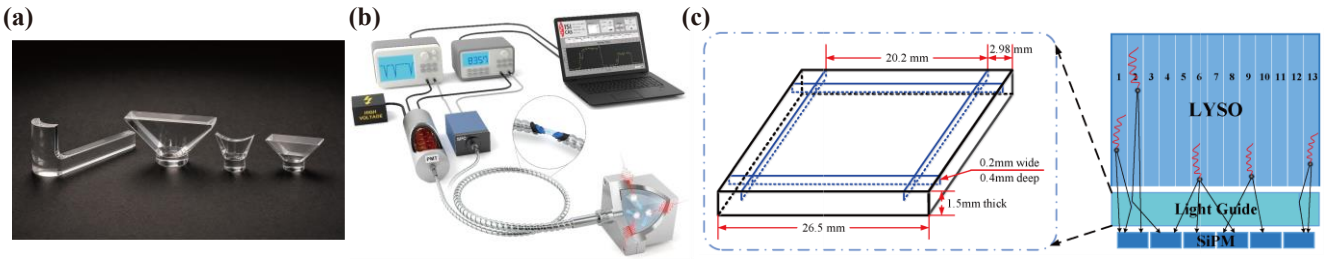

Figure 9. Application scenarios of light guides: **(a)** Light guides of various shapes manufactured by Eljen [104]; **(b)** Remote optical signal extraction and transmission using a scintillation fibre link [107]; **(c)** Light-guide matrix for optical signal mapping and multiplexed array readout [111]. Panel **(a)** was redrawn by the authors based on product photographs from Eljen Technology [104].

It should be noted that light guides introduce additional interfaces and optical path lengths. Improper design leads to light loss and time broadening, so their design must simultaneously satisfy optical, geometric, and reliability constraints [111,112].

Firstly, materials with good refractive index matching, high transmittance in the emission band, and low self-absorption should be selected. Meanwhile, internal bubbles, impurities, and defects should be controlled to reduce scattering and attenuation. Air gaps at the coupling interfaces between the scintillator, light guide, and detector should be eliminated during assembly. In terms of geometry, the cross-section transition of a light guide should be smooth, and abrupt shrinkage or sharp bending must be avoided [113]. This is because rapid cross-section reduction can break the total internal reflection condition and aggravate intrinsic light loss, with the loss generally becoming more severe as the reduction ratio increases. Some inorganic scintillation crystals (e.g., NaI: Tl, BGO) are highly brittle and fragile, so light guides can sometimes serve as a mechanical buffer layer between the PMT and the crystal [114]. For operation in environments with large temperature variations, the difference in thermal

expansion coefficients among the scintillator, optical adhesive, and light guide must be considered. Rigid coupling (e.g., cured optical adhesive) may fracture the crystal surface under thermal cycling. In such cases, non-curing optical silicone grease combined with a spring to provide moderate and constant compressive force is preferred.

5. Photodetector selection and matching

After the optimization of scintillator geometry, surface treatment, reflective layers, optical coupling media, and light-guide structures, the preceding sections have mainly focused on increasing the fraction of scintillation photons transported to the readout end, namely improving the LCE. The next assembly-level issue is whether these collected photons can be efficiently converted into measurable electrical signals. Therefore, photodetector selection and matching should be regarded as the terminal step of LCE-oriented optical-chain optimization rather than as an independent topic separated from LCE enhancement.

This section focuses on the selection and matching of photodetectors. Firstly, general criteria for photodetector selection are summarized from three aspects including spectral matching, geometric matching and parameter optimization. Then, the advantages, applicable scenarios and operational precautions of typical devices such as PMT, MCP-PMT and SiPM are compared. Combined with the light collection efficiency improvement strategies discussed previously, this section aims to complete the overall optimization chain by enhancing the conversion efficiency from collected photons into valid electrical signals.

5.1. General criteria for photodetector matching

5.1.1. Spectral matching between scintillator emission and detector response

Spectral matching is the primary basis for photodetector selection. Its core purpose is to make the main emission band of scintillators fall within the high-response region of photodetectors as far as possible, so as to improve the effective conversion probability of photons arriving at the readout end [50]. The spectral response of a photodetector describes the variation of its photoelectric conversion capability with incident light wavelength. For vacuum photodetectors such as PMTs and MCP-PMTs, spectral matching generally requires investigating entrance window transmittance and photocathode QE. The entrance window material mainly limits the short-wavelength transmission range, while the photocathode material determines the photoelectron emission probability, long-wavelength response range and QE peak position [115]. For SiPMs, spectral response is typically characterized by photon detection efficiency (PDE) curves. PDE is comprehensively influenced by light absorption in silicon, device structure, microcell fill factor and avalanche triggering probability [116]. Therefore, photodetector selection shall be based on the scintillator emission spectrum and compared with the wavelength-dependent response curves of target photodetectors. QE curves are generally taken as the main evaluation criterion for vacuum photodetectors, while PDE curves are used for SiPMs.

In addition to direct comparison of spectral curve overlap, spectral matching can also be characterized by quantitative calculation. Taking $LaBr_3$: Ce crystals and Hamamatsu H8500 series PMTs as research subjects, Scafe *et al.* [117] proposed the spectral matching factor (SMF) to evaluate the matching degree

between the scintillator emission spectrum S (λ) and the PMT quantum efficiency curve QE (λ). The SMF is defined as the ratio of their overlapping integral to the integral of the scintillator emission spectrum, which is essentially the normalized weighted average of PMT quantum efficiency over the scintillator emission spectrum. Its value ranges from 0 to 1. A value closer to 1 means a more sufficient overlap between the scintillator emission band and the high quantum efficiency region of the PMT, and the spectrally weighted effective response is closer to the peak response of the PMT. Furthermore, the effective quantum efficiency is expressed as $QE_{eff} = QE_{peak} \times SMF$, indicating that the actual photoelectric conversion performance of a photodetector relies on not only the peak quantum efficiency, but also the matching degree between the full emission spectrum and response spectrum. Similarly, QE (λ) can be substituted with PDE (λ) for SiPMs, and the effective PDE corresponding to a specific scintillator can be estimated by weighted averaging based on the scintillator emission spectrum. It can be concluded that in terms of spectral matching, photodetector selection should not only focus on peak QE or peak PDE values, but also pay attention to the effective overlap between the complete emission spectrum of scintillators and the spectral response of detectors.

5.1.2. Geometrical matching between the scintillator output face and sensitive area

Besides spectral matching, geometric matching also serves as an important criterion for photodetector selection. It mainly refers to the dimensional, morphological and spatial matching among scintillator light-emitting surface, light transmission path and effective sensitive area of photodetector. The effective sensitive area corresponds to the effective photocathode area of PMT, effective photosensitive area of SiPM, or effective pixel coverage of array detector.

It should be noted that geometric matching is not equivalent to a simple equality between the light exit area of scintillators and the detector area. Instead, it is necessary to verify whether the main outgoing light distribution modulated by coupling layers or light guides can be effectively covered by the detector. If the effective sensitive area is excessively large (Figure 10b), the signal can hardly be further enhanced, on the contrary, it will lead to increased dark noise, equivalent input capacitance, readout channel load and packaging cost. When the effective sensitive area is too small (Figure 10c), some photons cannot enter the photosensitive region, which further deteriorates energy resolution [118].

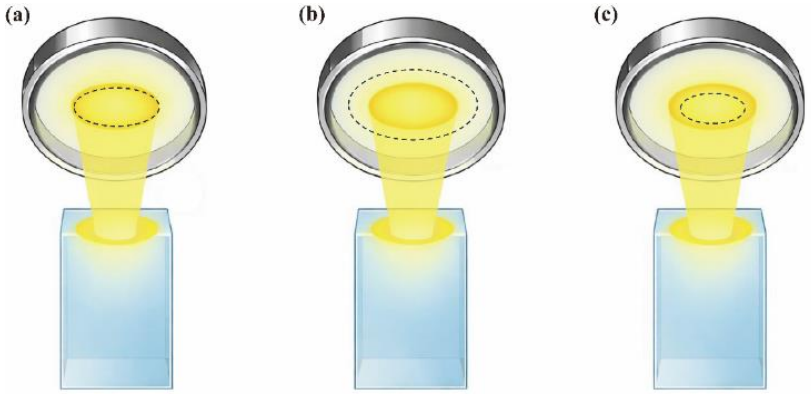

Figure 10. Geometrical matching between the scintillator output light distribution and the effective sensitive area of the photodetector: **(a)** Proper matching; **(b)** Oversized sensitive area; **(c)** Undersized sensitive area.

5.1.3. Application-dependent selection of photodetector parameters

After spectral and geometrical matching have been completed, further photodetector selection should be guided by the specific application requirements. Different scintillation detection systems impose different demands on the output signal; therefore, the suitability of a photodetector cannot be evaluated solely by a single parameter such as peak QE or PDE. From the perspective of assembly optimization, a more appropriate approach is to select the photodetector and its operating conditions according to the required energy resolution, timing resolution, count-rate capability, dynamic range, noise level, environmental adaptability, and long-term stability, on the basis that scintillation photons can effectively reach and cover the detector sensitive area. Table 2 summarizes the main parameter priorities for representative application scenarios.

Table 2. Application-dependent priorities for photodetector parameter selection.

Application target	Main selection priority	Typical detector consideration
Energy spectroscopy	Signal statistics and amplitude stability	High effective response, low noise, stable gain, good linearity
Fast timing/TOF	Timing precision	Low timing jitter, fast rise response, high prompt-photon sensitivity
High count rate	Linearity and rate capability	Wide dynamic range, low saturation risk, fast recovery
Weak-light or low-threshold detection	Noise suppression	Low dark signal, low false-count probability, stable threshold
Imaging or array readout	Integration density and channel uniformity	Suitable active area, pixel pitch, fill factor, manageable capacitance
Magnetic-field, portable, or harsh-environment	Environmental compatibility	Low-voltage operation, magnetic tolerance, temperature/radiation stability

5.2. Representative photodetectors for scintillation readout

5.2.1. Conventional dynode photomultiplier tubes

Photomultiplier tube (PMT) is a kind of vacuum photodetector working on the basis of external photoelectric effect. It is generally composed of an entrance window, photocathode, focusing electrodes, multistage dynodes and an anode (Figure 11a) [115]. Incident light passes through the window and generates photoelectrons on the photocathode. These photoelectrons are focused by electric field and multiplied via secondary electron emission in multistage dynodes, and electrical signals are eventually output from the anode. With high sensitivity, high gain and fast response speed, PMTs are especially suitable for detecting weak scintillation light signals, and are widely used in scintillation counting, gamma spectrum measurement, medical imaging, high energy physics, environmental monitoring and industrial inspection [119].

When selecting PMTs, good matching between the scintillator emission spectrum and the quantum efficiency curve of the device should be guaranteed first (Figure 11b) [120]. Insufficient overlap between the two spectra will result in a small number of initial photoelectrons, which degrades the signal-to-noise ratio and energy resolution even if the PMT has strong multiplication capacity. Then geometric matching should be considered. The effective photocathode area of PMT shall cover the main outgoing light distribution of the scintillator to the greatest extent. On this basis, further attention should be paid to

parameters such as dark current, gain stability, linear range, time response, maximum anode current and magnetic field sensitivity according to application demands. For example, energy spectrum measurement attaches more importance to low noise, stable gain and satisfactory linearity [121]; Rise time and transit time spread are prioritized for fast timing measurement and TOF detection [36]; For working conditions with high count rate or strong light output, it is essential to verify whether the PMT can sustain linear output characteristics [122].

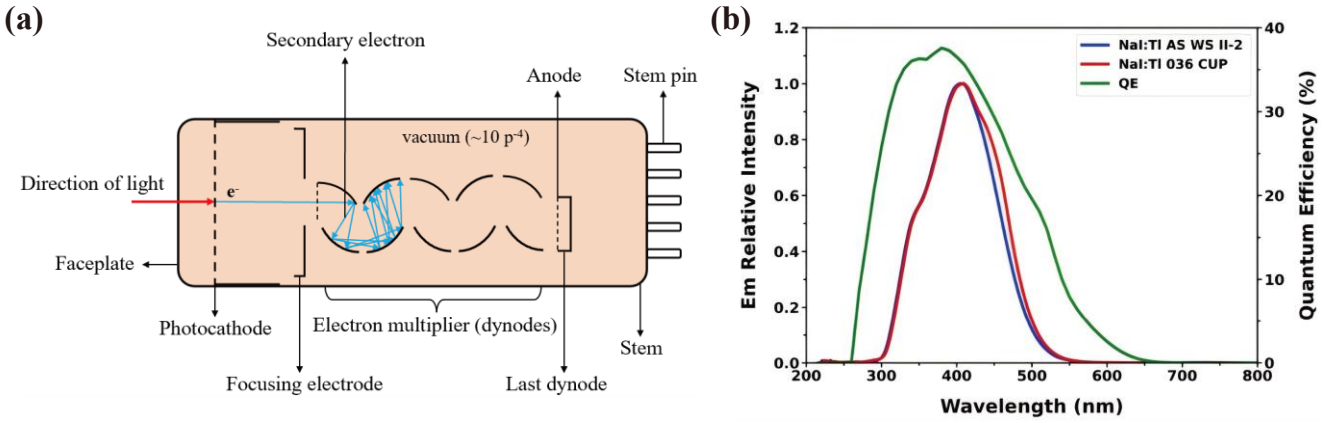

Figure 11. Representative photomultiplier tube structure and spectral matching: **(a)** Structure of a dynode photomultiplier tube [115]; **(b)** Comparison between the X-ray induced emission of NaI: Tl crystals and the quantum efficiency of the photomultiplier tube [120]. Reprinted with permission from [120]. Copyright 2025 IOP Publishing. Panel **(a)** was redrawn by the authors based on the structural descriptions in [115].

5.2.2. Microchannel-plate photomultiplier tubes

MCP-PMTs use microchannel plates (MCPs) instead of the conventional dynode multiplication chain. Their typical structure consists of an entrance window, photocathode, MCP, and anode, with a photocathode-to-MCP distance of approximately 2 mm, forming a proximity-focusing configuration (Figure 12a) [115,123]. To achieve sufficient gain, two or more stacked MCPs are often employed, and an ion-barrier film is introduced at the input to suppress ion-feedback damage to the photocathode [115,124,125]. This structure enables the application of a nearly uniform parallel electric field between the photocathode and MCP as well as between the MCP and anode, thereby reducing the influence of the initial emission angle and initial velocity on electron transit. In addition, the extremely short multiplication path within the MCP significantly shortens the transit time, making MCP-PMTs among the best-performing vacuum photoelectric devices in terms of temporal response. Taking the Hamamatsu R3809U-50 as an example, the TTS can reach 25 ps when evaluated using a 5-ps (FWHM) laser, making it suitable for extreme timing applications such as TOF and fast coincidence counting (Figure 12b) [115,126]. It should also be noted that its magnetic-field tolerance is highly directional: it can operate up to approximately 2.0 T when the magnetic field is parallel to the tube axis, whereas the output decreases significantly when the magnetic field is perpendicular to the tube axis and exceeds approximately 70 mT. Therefore, both device selection and installation should be designed with the magnetic-field orientation in mind [115].

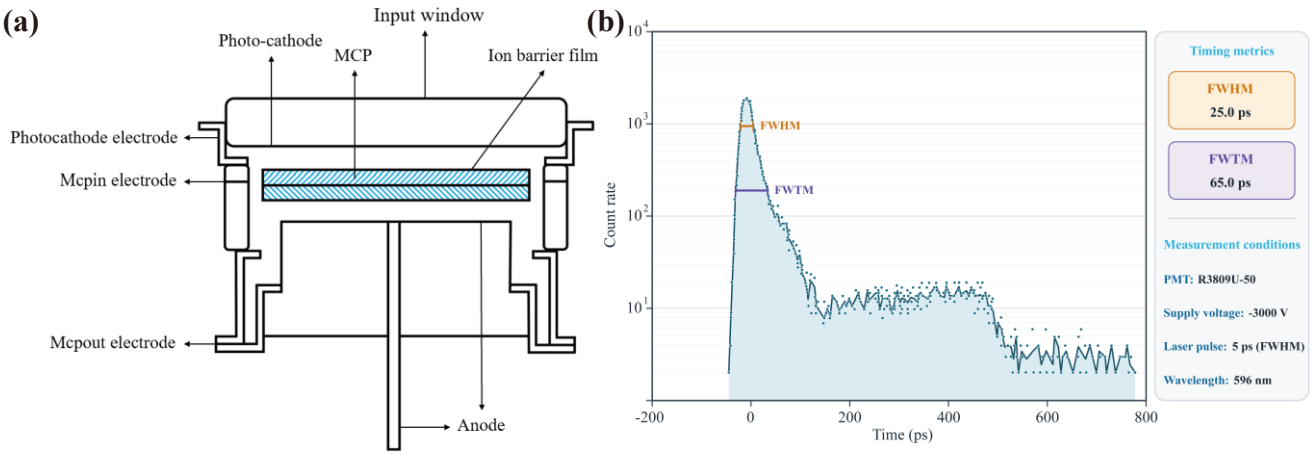

Figure 12. Structure and key performance features of MCP-PMTs for fast scintillation readout: **(a)** Schematic cross-section of an MCP-PMT structure [115]; **(b)** Measurement of T.T.S. for MCP-PMT [115]. Panels **(a)** and **(b)** were redrawn by the authors based on the structural descriptions and data reported in [115].

5.2.3. Silicon photomultipliers

Silicon photomultipliers (SiPMs) are solid-state photodetectors composed of many Geiger-mode microcells connected in parallel (Figure 13a,b) [127,128]. Compared with conventional photomultiplier tubes, SiPMs offer low operating voltage, compact size, fast response, high integration density, and insensitivity to magnetic fields. These advantages make them suitable for compact scintillation detectors, PET detector modules, portable radiation instruments, and pixelated or array-based readout systems [116]. More detailed discussions of SiPM fundamentals and performance parameters can be found in the review by Gundacker and Heering [129].

For SiPM-based scintillation readout, the PDE spectrum should first be matched with the main emission band of the scintillator (Figure 13c). PDE represents the probability that an incident photon produces a detectable avalanche signal and is mainly determined by quantum efficiency, microcell fill factor, and avalanche triggering probability [116]. In addition to spectral matching, geometrical matching and dynamic range are particularly important. Since each fired microcell produces a nearly fixed-amplitude pulse, the SiPM output depends on the number of fired microcells within the signal integration time. When many photons arrive within a short time window, the finite number of available microcells may cause saturation and nonlinear response (Figure 13d) [130–132]. This issue is especially important for high-light-yield scintillators, efficient optical coupling structures, or small-area SiPMs. Therefore, SiPM active area, microcell size, microcell density, and recovery time should be selected according to the expected photon flux.

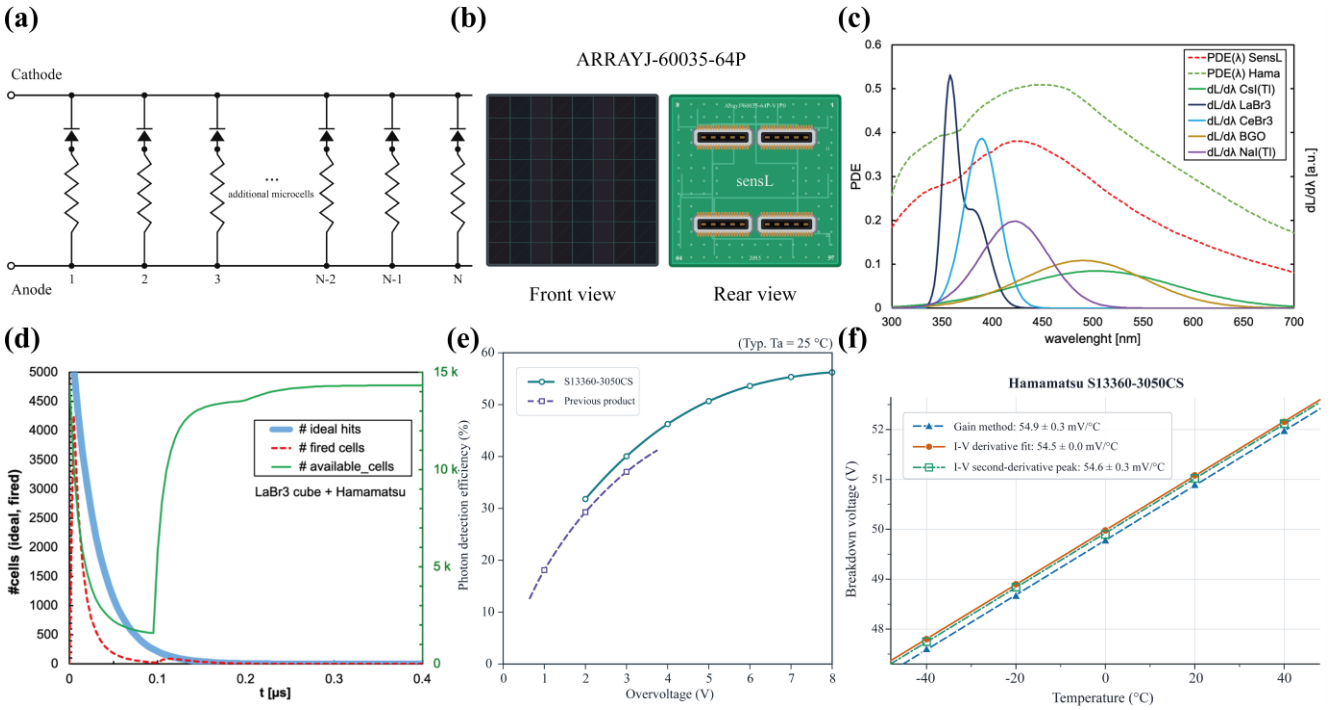

Figure 13. Structural features, spectral matching, and operational constraints of SiPMs for scintillation readout: **(a)** Equivalent circuit of a SiPM microcell array [127]; **(b)** Representative SiPM and array modules [128]; **(c)** Spectral overlap between scintillator emission spectra and SiPM PDE curves [130]; **(d)** Time evolution of ideal hits, fired microcells, and available microcells, illustrating saturation and nonlinear response under high instantaneous photon flux [130]; **(e)** Dependence of photon detection efficiency on overvoltage [116]; **(f)** Breakdown voltage-temperature curve for the Hamamatsu S13360-3050CS [133]. Panels **(a)**, **(b)**, **(e)** and **(f)** were redrawn by the authors based on the data, equivalent-circuit descriptions, and product information reported in [116,127,128,133].

The SiPM operating point also requires careful control. Increasing overvoltage generally improves gain, avalanche triggering probability, and PDE (Figure 13e), but it also increases dark count rate, optical crosstalk, and afterpulsing. In addition, the breakdown voltage of SiPMs is temperature dependent. If the bias voltage is kept constant, temperature variation changes the effective overvoltage (Figure 13f), thereby affecting gain, PDE, noise, crosstalk, and afterpulsing [116]. Therefore, temperature compensation, bias-voltage adjustment, or gain correction is often required to maintain stable detector response [134,135].

6. AI-assisted design and optimization of scintillation detector assembly

The assembly optimization of scintillation detectors is a highly coupled multi-parameter problem. Scintillator geometry, surface treatment, reflector configuration, coupling medium, light-guide design, and photodetector matching jointly influence LCE, light-output uniformity, photon transit-time distribution, energy resolution, and timing performance. These parameters are not independent: for example, a strategy that increases light extraction may also broaden the photon arrival-time distribution, while a reflector or coupling scheme that improves light output may compromise packing density, mechanical reliability, or long-term stability. Therefore, LCE-oriented assembly optimization should be regarded as a multi-objective design problem rather than the maximization of a single optical parameter.

Monte Carlo optical-photon tracking based on tools such as Geant4 and GATE can describe photon generation, reflection, refraction, absorption, scattering, and detector coupling in detail [136,137]. However, when realistic surface models, wavelength-dependent reflectors, coupling layers, light guides, and photodetector responses are considered simultaneously, exhaustive parameter scanning becomes computationally expensive. In this context, AI-assisted methods can act as an intermediate layer between physics-based simulation and experimental validation. Instead of replacing optical simulation, machine-learning models can be trained as surrogate models to approximate the relationship between assembly descriptors and detector performance, thereby accelerating sensitivity analysis, parameter screening, and design iteration. Figure 14 illustrates the AI-assisted workflow for scintillation detector assembly optimization, where Monte Carlo simulations and experimental data are used to build surrogate models for predicting detector performance, followed by multi-objective optimization to identify optimal assembly configurations.

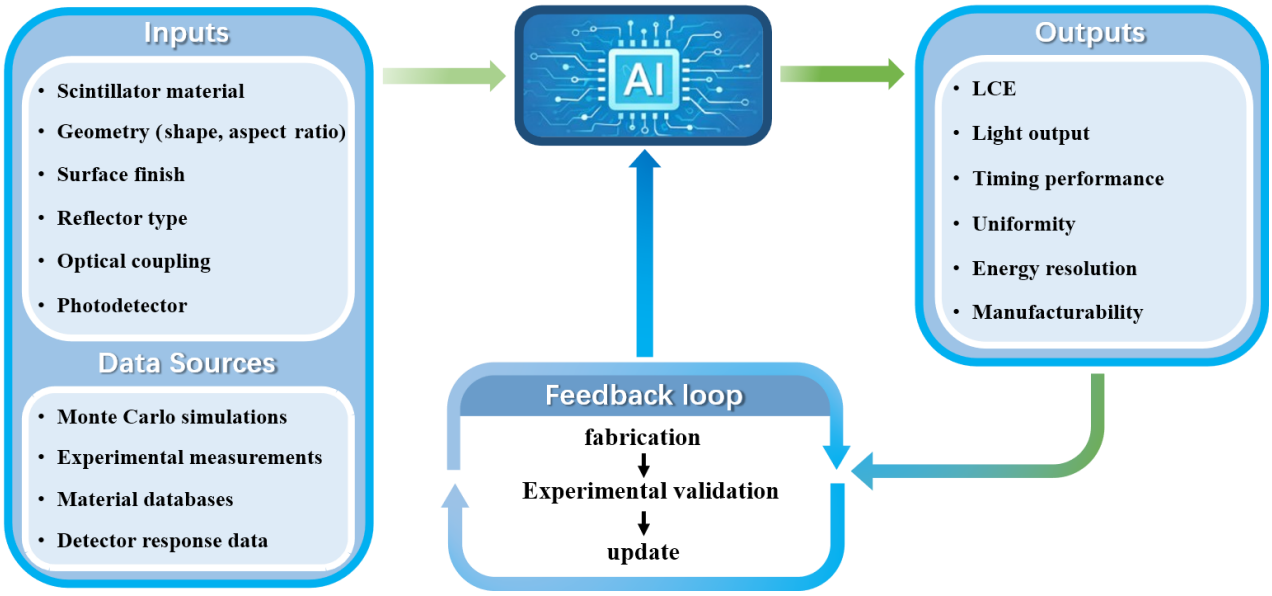

Figure 14. AI-assisted workflow for assembly optimization of scintillation detectors.

A practical AI-assisted workflow may include four steps. First, hybrid datasets are generated from Monte Carlo simulations and selected calibration experiments. The input descriptors may include crystal size, aspect ratio, taper angle, surface finish, reflector type and thickness, coupling-medium refractive index, coupling-layer thickness, light-guide geometry, and photodetector spectral response. The output metrics may include LCE, detected signal yield, light-output uniformity, photon transit-time spread, and proxies for energy or timing resolution. Second, surrogate models are trained to predict these performance metrics from assembly parameters. Third, multi-objective optimization or inverse design is used to identify assembly configurations that balance LCE, timing response, uniformity, packing density, manufacturability, and stability. Finally, the predicted optimal assemblies are fabricated and experimentally validated, and the deviations between prediction and measurement are fed back to update the simulation and surrogate models.

At present, AI-driven assembly optimization for scintillation detectors should still be considered a forward-looking workflow rather than a mature standardized methodology. Most existing AI studies in scintillator-based detectors focus on event positioning, timing estimation, response reconstruction, or

uncertainty-aware signal analysis, rather than direct optimization of assembly parameters. For example, neural-network-based methods have been used to infer gamma-interaction positions or timestamps from light distributions in monolithic or semi-monolithic scintillator detectors [138–140]. Although these studies do not directly optimize the assembly structure, they demonstrate that complex scintillation-light transport patterns contain learnable high-dimensional information. In addition, emulator-based Bayesian inference and uncertainty-aware deep-learning reconstruction show that surrogate or physics-guided models can be useful when direct computation is expensive and detector response is strongly coupled [141,142].

Therefore, the near-term role of AI in scintillation detector assembly is most credible as simulation-accelerated and experimentally calibrated optimization. AI can reduce the cost of large parameter scans, identify critical assembly variables, and support multi-objective design decisions. However, experimental feedback remains essential because practical assembly involves polishing nonuniformity, reflector attachment defects, coupling-layer thickness variation, trapped bubbles, adhesive shrinkage, aging, yellowing, and detector-to-detector variation. As standardized simulation datasets and experimentally validated assembly data become available, AI-assisted design may become an effective tool for transferable and application-specific LCE optimization.

7. Conclusion and outlook

Light collection efficiency is a key intermediate variable that connects the intrinsic scintillation capability of a material with the final measurable performance of a detector. Although scintillation yield determines the upper limit of photon generation, the fraction of photons that can be effectively extracted, transported, and converted into measurable electrical signals is largely governed by assembly-level design. Therefore, scintillation-detector performance should be understood not only as a material issue, but also as the result of coordinated optimization across the entire optical chain.

This review has summarized the principal assembly factors affecting LCE, including scintillator selection, geometrical design, surface treatment, reflector configuration, optical coupling, light-guide engineering, and photodetector matching. Existing studies show that these factors are strongly interdependent: material properties define the initial photon-generation conditions, geometry and surface treatment regulate photon transport, reflector and coupling systems determine interface recycling and transmission, and photodetector matching controls the final utilization of collected photons. Rational assembly optimization can therefore improve light output, energy resolution, timing performance, and response uniformity. However, many reported strategies remain material- or application-specific, and improvements in one metric may compromise others.

Future research should move from empirical optimization toward quantitative and application-oriented design rules. In particular, more attention should be paid to cross-scale coupling mechanisms among material properties, optical transport, interface conditions, and detector response. As scintillation detectors continue to evolve toward compact integration, array readout, high count-rate operation, and harsh-environment deployment, multi-objective optimization will become increasingly important. AI-assisted methods, when combined with optical simulation and experimental validation, may provide useful tools for exploring complex assembly parameter spaces and accelerating LCE-oriented detector design. Overall, assembly optimization provides an important pathway for translating the intrinsic advantages of scintillation materials into practical high-performance detection systems.

Declaration of generative AI and AI-assisted technologies

During the preparation of this work, the authors used ChatGPT for language polishing and text refinement. After using this tool, the authors reviewed and edited the content as needed and take full responsibility for the content of the publication.

Acknowledgments

This work was supported by the National Key Research and Development Program of China (No. 2022YFB1902700); Joint Fund for Equipment Pre-research of the Ministry of Education of the People's Republic of China (No. 8091B042203); National Natural Science Foundation of China (Nos. 11875129 and 12405217); Natural Science Foundation of Shandong Province (No. ZR202211030043); Fund of National Key Laboratory of Plasma Physics (No. 6142A04240203); Fund of State Key Laboratory of Intense Pulsed Radiation Simulation and Effect (No. SKLIPR1810); Fund of State Key Laboratory of Nuclear Physics and Technology of Peking University (No. NPT2023KFY06); State Key Laboratory of Crystal Materials, Shandong University (No. KF2401); and Fundamental Research Funds for the Central Universities (Nos. 2025JG002 and 2025MS059).

Authors' contribution

Conceptualization, Yuze Hua, Xuesong Li and Yang Liu; methodology, Yuze Hua; investigation, Yuze Hua; resources, Yuze Hua, Xuxin Yang and Jinzhu Chen; data curation, Yuze Hua; formal analysis, Yuze Hua; visualization, Yuze Hua; writing—original draft preparation, Yuze Hua; writing—review and editing, Yuze Hua, Xuxin Yang, Jinzhu Chen, Xuesong Li and Yang Liu; supervision, Xuesong Li and Yang Liu; project administration, Xuesong Li and Yang Liu; funding acquisition, Xuesong Li and Yang Liu. All authors have read and agreed to the published version of the manuscript.

Conflicts of interest

The authors declare no conflicts of interest.

References

[1] Gao Q, Wang Q, Ran P, Buryi M, Yang J, *et al.* Boosting scintillation yield in $Cs_3Cu_2I_5$ single crystals via europium (II) incorporation toward high-resolution and fast X-ray imaging. *Laser Photonics Rev.* 2026, 20(1):e01596.

[2] Zhou Q, Li W, Xiao J, Li A, Han X. Low-dimensional metal halide for high performance scintillators. *Adv. Funct. Mater.* 2024, 34(38):2402902.

[3] Zhu D, Nikl M, Chewpraditkul W, Li J. Development and prospects of garnet ceramic scintillators: a review. *J. Adv. Ceram.* 2022, 11(12):1825–1848.

[4] Bortfeldt J, Brunbauer F, David C, Desforge D, Fanourakis G, *et al.* Timing performance of a micro-channel-plate photomultiplier tube. *Nucl. Instrum. Methods Phys. Res. Sect. A* 2020, 960:163592.

[5] Park H, Yi M, Lee JS. Silicon photomultiplier signal readout and multiplexing techniques for positron emission tomography: a review. *Biomed. Eng. Lett.* 2022, 12(3):263–283.

[6] Régis JM, Fraile LM, Rudigier M. γ-γ fast timing with high-performance LaBr3 (Ce) scintillators. *Prog. Part. Nucl. Phys.* 2025, 141:104152.

[7] Gonzalez-Montoro A, Ullah MN, Levin CS. Advances in detector instrumentation for PET. *J. Nucl. Med.* 2022, 63(8):1138–1144.

[8] Dujardin C, Auffray E, Bourret-Courchesne E, Dorenbos P, Lecoq P, *et al.* Needs, trends, and advances in inorganic scintillators. *IEEE Trans. Nucl. Sci.* 2018, 65(8):1977–1997.

[9] Wang Z, Dujardin C, Freeman MS, Gehring AE, Hunter JF, *et al.* Needs, trends, and advances in scintillators for radiographic imaging and tomography. *IEEE Trans. Nucl. Sci.* 2023, 70(7):1244–1280.

[10] Trigila C, Roncali E. Optimization of scintillator-reflector optical interfaces for the LUT Davis model. *Med. Phys.* 2021, 48(9):4883–4899.

[11] Hull G, Du S, Niedermayr T, Payne S, Cherepy N, *et al.* Light collection optimization in scintillator-based gamma-ray spectrometers. *Nucl. Instrum. Methods Phys. Res. Sect. A* 2008, 588(3):384–388.

[12] Singh P, Dosovitskiy G, Bekenstein Y. Bright innovations: review of next-generation advances in scintillator engineering. *ACS Nano* 2024, 18(22):14029–14049.

[13] Birks JB. *The Theory and Practice of Scintillation Counting: International Series of Monographs in Electronics and Instrumentation*. Amsterdam: Elsevier, 2013.

[14] Janecek M, Moses WW. Simulating scintillator light collection using measured optical reflectance. *IEEE Trans. Nucl. Sci.* 2010, 57(3):964–970.

[15] Knoll GF. *Radiation Detection and MEASUrement*. Hoboken: John Wiley & Sons, 2010.

[16] Mottaghian M, Koohi-Fayegh R, Ghal-Eh N, Etaati GR. Photocathode non-uniformity contribution to the energy resolution of scintillators. *Radiat. Prot. Dosim.* 2010, 140(1):16–24.

[17] Kurman Y, Shultzman A, Segal O, Pick A, Kaminer I. Photonic-crystal scintillators: molding the flow of light to enhance X-ray and γ-ray detection. *Phys. Rev. Lett.* 2020, 125(4):040801.

[18] Danevich FA, Kobychev VV, Kobychev RV, Kraus H, Mikhailik VB, *et al.* Impact of geometry on light collection efficiency of scintillation detectors for cryogenic rare event searches. *Nucl. Instrum. Methods Phys. Res. Sect. B*. 2014, 336:26–30.

[19] Roncali E, Stockhoff M, Cherry SR. An integrated model of scintillator-reflector properties for advanced simulations of optical transport. *Phys. Med. Biol.* 2017, 62(12):4811–4830.

[20] Ayotte G, Archambault L, Gingras L, Lacroix F, Beddar AS, *et al.* Surface preparation and coupling in plastic scintillator dosimetry. *Med. Phys.* 2006, 33(9):3519–3525.

[21] Yanagida T. Inorganic scintillating materials and scintillation detectors. *Proc. Jpn. Acad. Ser. B Phys. Biol. Sci.* 2018, 94(2):75–97.

[22] Sosa CS, Thompson SJ, Chichester DL, Clarke SD, Di Fulvio A, *et al.* Energy resolution experiments of conical organic scintillators and a comparison with Geant4 simulations. *Nucl. Instrum. Methods Phys. Res. Sect. A* 2018, 898:77–84.

[23] Moszyński M, Syntfeld-Każuch A, Swiderski L, Grodzicka M, Iwanowska J, *et al.* Energy resolution of scintillation detectors. *Nucl. Instrum. Methods Phys. Res. Sect. A* 2016, 805:25–35.

[24] Katrunov K, Ryzhikov V, Gavrilyuk V, Naydenov S, Lysetska O, *et al.* Optimum design calculations for detectors based on ZnSe (Te, O) scintillators. *Nucl. Instrum. Methods Phys. Res. Sect. A* 2013, 712:126–129.

[25] Su C, Liu Q, Kong L, Chen S, Moharrami K, *et al.* Characterization and optimization of a cryogenic pure CsI detector with remarkable light yield and unprecedented energy resolution for CLOVERS experiment. *Nucl. Sci. Tech.* 2025, 36(5):82.

[26] Sertore D, Michelato P, Monaco L, Pagani C. A study for the characterization of high QE photocathodes. In *Proceedings of the 2007 IEEE Particle Accelerator Conference*, Albuquerque, USA, June 25–29, 2007, pp. 2760–2762.

[27] Fraser-Mitchell J, Wright AG. Contribution of photocathode nonuniformity to energy resolution in NaI (Tl) scintillation detectors. *Nucl. Instrum. Methods Phys. Res. Sect. A* 1990, 288(2–3):429–438.

[28] Yasuda K, Usuda S, Gunji H. Properties of a YAP powder scintillator as alpha-ray detector. *Appl. Radiat. Isot.* 2000, 52(3):365–368.

[29] Lee SK, Kang SY, Jang DY, Lee CH, Kang SM. Comparison of new simple methods in fabricating ZnS (Ag) scintillators for detecting alpha particles. *Prog. Nucl. Sci. Technol.* 2011, 1:194–197.

[30] Morishita Y, Hoshi K, Torii T. Evaluation of an ultra-thin plastic scintillator to detect alpha and beta particle contamination. *Nucl. Instrum. Methods Phys. Res. Sect. A* 2020, 966:163795.

[31] Van Pelt WR, Drzyzga M. Beta radiation shielding with lead and plastic: effect on bremsstrahlung radiation when switching the shielding order. *Health Phys.* 2007, 92(2):S13–S17.

[32] An B, Deng Y, Jin Z, Sun S. Scintillators for neutron detection and imaging: advances and prospects. *Adv. Funct. Mater.* 2025, 35(19):2422522.

[33] Sykora GJ, Mann SE, Mauri G, Schooneveld EM, Rhodes NJ. Review of thermal neutron scintillators: evaluation metrics and future prospects for demanding applications. *Opt. Mater. X* 2024, 24:100373.

[34] Kumar DA, Parthiban E. Recent advancements of organic scintillators in enhancing the performance of fast neutron detection: a review. *Nucl. Anal.* 2025, 4(2):100171.

[35] Huang T, Fu Q, Lin S, Wang B. NaI (Tl) scintillator read out with SiPM array for gamma spectrometer. *Nucl. Instrum. Methods Phys. Res. Sect. A* 2017, 851:118–124.

[36] Vandenberghe S, Mikhaylova E, D'Hoe E, Mollet P, Karp JS. Recent developments in time-of-flight PET. *EJNMMI Phys.* 2016, 3(1):3.

[37] Shah KS, Glodo J, Klugerman M, Moses WW, Derenzo SE, *et al.* LaBr3: Ce scintillators for gamma-ray spectroscopy. *IEEE Trans. Nucl. Sci.* 2003, 50(6):2410–2413.

[38] Koshimizu M. Recent progress of organic scintillators. *Jpn. J. Appl. Phys.* 2023, 62(1):010503.

[39] Salomoni M, Pots R, Auffray E, Lecoq P. Enhancing light extraction of inorganic scintillators using photonic crystals. *Crystals* 2018, 8(2):78.

[40] Sasano M, Nishioka H, Okuyama S, Nakazawa K, Makishima K, *et al.* Geometry dependence of the light collection efficiency of BGO crystal scintillators read out by avalanche photo diodes. *Nucl. Instrum. Methods Phys. Res. Sect. A* 2013, 715:105–111.

[41] Carrier C, Lecomte R. Effect of geometrical modifications and crystal defects on light collection in ideal rectangular parallelepipedic BGO scintillators. *Nucl. Instrum. Methods Phys. Res. Sect. A* 1990, 294(1–2):355–364.

[42] Perez-Benito D, Chil R, Hidalgo-Torres LA, Vaquero JJ. Scintillator geometrical considerations for detectors based on hexagonal sipms. *IEEE Trans. Radiat. Plasma Med. Sci.* 2023, 7(7):684–691.

[43] Senchyshyn V, Lebedev V, Adadurov A, Budagov J, Chirikov-Zorin I. Accounting for self-absorption in calculation of light collection in plastic scintillators. Nucl. Instrum. *Methods Phys. Res. Sect. A* 2006, 566(2):286–293.

[44] Wei Y, Zhang Z, Zhang Y, Wang C, Wen S, *et al.* Performance of the BGO detector element of the DAMPE calorimeter. *IEEE Trans. Nucl. Sci.* 2016, 63(2):548–551.

[45] Pauwels K, Auffray E, Gundacker S, Knapitsch A, Lecoq P. Effect of aspect ratio on the light output of scintillators. *IEEE Trans. Nucl. Sci.* 2012, 59(5):2340–2345.

[46] Katrunov K, Ryzhikov V, Gavrilyuk V, Naydenov S, Lysetska O, *et al.* Optimum design calculations for detectors based on ZnSe (Te, O) scintillators. *Nucl. Instrum. Methods Phys. Res. Sect. A* 2013, 712:126–129.

[47] Danevich FA, Kobychev RV, Kobychev VV, Kraus H, Mikhailik VB, *et al.* Optimization of light collection from crystal scintillators for cryogenic experiments. *Nucl. Instrum. Methods Phys. Res. Sect. A* 2014, 744:41–47.

[48] Sosa CS, Thompson SJ, Chichester DL, Clarke SD, Di Fulvio A, *et al.* Energy resolution experiments of conical organic scintillators and a comparison with Geant4 simulations. *Nucl. Instrum. Methods Phys. Res. Sect. A* 2018, 898:77–84.

[49] Sosa CS, Thompson SJ, Chichester DL, Schuster PF, Clarke SD, *et al.* Improved neutron–gamma discrimination at low-light output events using conical trans-stilbene. *Nucl. Instrum. Methods Phys. Res. Sect. A* 2019, 916:42–46.

[50] Roncali E, Mosleh-Shirazi MA, Badano A. Modelling the transport of optical photons in scintillation detectors for diagnostic and radiotherapy imaging. *Phys. Med. Biol.* 2017, 62(20):R207–R235.

[51] Xie S, Sun Q, Ying G, Guo L, Huang Q, *et al.* Ultra-precise surface processing of LYSO scintillator crystals for positron emission tomography. *Appl. Surf. Sci.* 2019, 469:573–581.

[52] Nicodemus FE, Richmond JC, Hsia JJ, Ginsberg IW, Limperis T. *Geometrical Considerations and Nomenclature for Reflectance*. Washington: National Bureau of Standards, 1977. pp. 1–52.

[53] Xie S, Zhang X, Zhang Y, Ying G, Huang Q, *et al.* Evaluation of various scintillator materials in radiation detector design for positron emission tomography (PET). *Crystals* 2020, 10(10):869.

[54] McMillan JE. Improvements to light collection in scintillation detectors intended for fast cosmic ray timing. In *Proceedings of the 29th International Cosmic Ray Conference*, Pune, India, 2005, pp. 283–286.

[55] Kolcu OB, Iren E, Yetkin T, Özok F, Erduran MN. Measurement of LYSO crystal light output and energy resolution improvement with acid etching. *Appl. Radiat. Isot.* 2023, 199:110902.

[56] Jeong DW, Choi E, Cho JY, Luan NT, Park H, *et al.* Optimization of scintillation light collection efficiency in BGO crystals with surface diffusion for enhanced sensitivity in the KAPAE. *IEEE Trans. Nucl. Sci.* 2025, 72(7):2071–2075.

[57] Yang F, Zhang L, Zhu R. Monitoring LSO/LYSO crystal calorimeters. *IEEE Trans. Nucl. Sci.* 2016, 63(2):605–611.

[58] Spanoudaki VC, Levin C. Investigating the temporal resolution limits of scintillation detection from pixellated elements: comparison between experiment and simulation. *Phys. Med. Biol.* 2011, 56(3):735–756.

[59] Vilardi I, Braem A, Chesi E, Ciocia F, Colonna N, *et al.* Optimization of the effective light attenuation length of YAP: Ce and LYSO: Ce crystals for a novel geometrical PET concept. *Nucl. Instrum. Methods Phys. Res. Sect. A* 2006, 564(1):506–514.

[60] Jung JH, Choi Y, Yun J, Jung J, Lee S. Effects of reflector, surface treatment, and length of scintillation crystal on the performance of TOF-DOI PET detector with dual-ended readout. *Nucl. Eng. Technol.* 2024, 56(7):2633–2640.

[61] Gramuglia F, Frasca S, Ripiccini E, Venialgo E, Gâté V, *et al.* Light extraction enhancement techniques for inorganic scintillators. *Crystals* 2021, 11(4):362.

[62] Trigila C, Roncali E. Effect of crystal-photodetector interface extraction efficiency on Cerenkov photons' detection time. *Front. Phys.* 2022, 10:1028293.

[63] Moses WW, Choong WS, Derenzo SE. Modeling time dispersion due to optical path length differences in scintillation detectors. *Acta Phys. Pol. B Proc. Suppl.* 2014, 7(4):725.

[64] Auffray E, Frisch B, Geraci F, Ghezzi A, Gundacker S, *et al.* A comprehensive & systematic study of coincidence time resolution and light yield using scintillators of different size and wrapping. *IEEE Trans. Nucl. Sci.* 2013, 60(5):3163–3171.

[65] Salomoni M, Pots R, Auffray E, Lecoq P. Enhancing light extraction of inorganic scintillators using photonic crystals. *Crystals* 2018, 8(2):78.

[66] Kronberger M, Auffray E, Lecoq PR. Improving light extraction from heavy inorganic scintillators by photonic crystals. *IEEE Trans. Nucl. Sci.* 2010, 57(5):2475–2482.

[67] Zhu Z, Liu B, Zhang H, Ren W, Cheng C, *et al.* Improvement of light extraction of LYSO scintillator by using a combination of self-assembly of nanospheres and atomic layer deposition. *Opt. Express* 2015, 23(6):7085–7093.

[68] Heinrichs U, Blume A, Bussmann N, Engels R, Kemmerling G, *et al.* Statistical studies on the light output and energy resolution of small LSO single crystals with different surface treatments combined with various reflector materials. *Nucl. Instrum. Methods Phys. Res. Sect. A* 2002, 486(1–2):60–66.

[69] Wan Q, Wang Q, Xie Y, Xiao X, Zhang Z, *et al.* Study on packaging technology of GAGG: Ce scintillation detector. *At. Energy Sci. Technol.* 2025, 59(1):183–188.

[70] Roncali E, Cherry SR. Simulation of light transport in scintillators based on 3D characterization of crystal surfaces. *Phys. Med. Biol.* 2013, 58(7):2185–2198.

[71] Li X, Ruiz-Gonzalez M, Furenlid LR. An edge-readout, multilayer detector for positron emission tomography. *Med. Phys.* 2018, 45(6):2425–2438.

[72] Beheshti A, Karimian A, Arabi H, Goertzen AL. A new design to improve time resolution in a time of flight brain PET using dual layer offset scintillator crystals. *Sci. Rep.* 2025, 15(1):15634.

[73] Gundacker S, Knapitsch A, Auffray E, Jarron P, Meyer T, *et al.* Time resolution deterioration with increasing crystal length in a TOF-PET system. *Nucl. Instrum. Methods Phys. Res. Sect. A* 2014, 737:92–100.

[74] Huber JS, Moses WW, Andreaco MS, Loope M, Melcher CL, *et al.* Geometry and surface treatment dependence of the light collection from LSO crystals. *Nucl. Instrum. Methods Phys. Res. Sect. A* 1999, 437(2–3):374–380.

[75] Knapitsch A, Lecoq P. Review on photonic crystal coatings for scintillators. *Int. J. Mod. Phys. A* 2014, 29(30):1430070.

[76] Janecek M. Reflectivity spectra for commonly used reflectors. *IEEE Trans. Nucl. Sci.* 2012, 59(3):490–497.

[77] Park K, Cho S, Franca LE, Ha CH, Kim J, *et al.* Validation of the COSINE-100U NaI(Tl) encapsulation for low-temperature operation in liquid scintillator. *arXiv* 2026, arXiv:2601.12819.

[78] Janecek M, Moses WW. Measuring light reflectance of BGO crystal surfaces. *IEEE Trans. Nucl. Sci.* 2008, 55(5):2443–2449.

[79] Rakić AD, Djurišić AB, Elazar JM, Majewski ML. Optical properties of metallic films for vertical-cavity optoelectronic devices. *Appl. Opt.* 1998, 37(22):5271–5283.

[80] Weidner VR, Hsia JJ. Reflection properties of pressed polytetrafluoroethylene powder. *J. Opt. Soc. Am.* 1981, 71(7):856–861.

[81] Gichaba JO. Measurements of TYVEK reflective properties for the Pierre auger project. Master's Thesis, The University of Mississippi, 1998.

[82] Labsphere, Inc. Reflectance coatings and materials TechGuide (Rev 04). 2024. Available: https://www.labsphere.com (accessed on 7 March 2026).

[83] The Chemours Company FC, LLC. Ti-Pure™ titanium dioxide for coatings. 2019. Available: https://www.tipure.com (accessed on 7 March 2026).

[84] Budde W. Calibration of reflectance standards. *J. Res. Natl. Bur. Stand. Sect. A Phys. Chem.* 1976, 80(4):585.

[85] Pozzobon V, Levasseur W, Do KV, Palpant B, Perre P. Household aluminum foil matte and bright side reflectivity measurements: application to a photobioreactor light concentrator design. *Biotechnol. Rep.* 2020, 25:e00399.

[86] 3M Company. 3M™ Enhanced Specular Reflector Films (3M™ ESR) Technical Data Sheet (R2). 2021. Available: https://www.3m.com/displayenhancement (accessed on 7 March 2026).

[87] Pepin CM, Bérard P, Lecomte R. Assessment of reflective separator films for small crystal arrays. In *Proceedings of 2001 IEEE Nuclear Science Symposium Conference Record*, San Diego, USA, November 2001, pp. 879–883.

[88] Kuang Z, Wang X, Fu X, Ren N, Yang Q, *et al.* Dual-ended readout small animal PET detector by using 0.5 mm pixelated LYSO crystal arrays and SiPMs. *Nucl. Instrum. Methods Phys. Res. Sect. A* 2019, 917:1–8.

[89] Zatcepin A, Pizzichemi M, Polesel A, Paganoni M, Auffray E, *et al.* Improving depth-of-interaction resolution in pixellated PET detectors using neural networks. *Phys. Med. Biol.* 2020, 65(17):175017.

[90] Du J, Du S. Performance comparison of DOI-encoding PET detectors based on 1.1-mm pitch BGO arrays with different reflectors. *IEEE Trans. Radiat. Plasma Med. Sci.* 2024, 8(3):257–262.

[91] 3M Company. Vikuiti™ Enhanced Specular Reflector (ESR). 2005. Available: https://www.3M.com/Vikuiti (accessed on 7 March 2026).

[92] Felicelli A, Wang J, Feng D, Forti E, El Awad Azrak S, *et al.* Efficient radiative cooling of low-cost BaSO4 paint-paper dual-layer thin films. *Nanophotonics* 2024, 13(5):639–648.

[93] El-Tayebany RA. Characterization of wrapping and coating techniques for light-reflecting materials of LaBr3 (Ce) scintillation detector. *Sci. Rep.* 2025, 15(1):16835.

[94] Gonzalez-Montoro A, Pourashraf S, Lee MS, Cates JW, Levin CS. Study of optical reflectors for a 100 ps coincidence time resolution TOF-PET detector design. *Biomed. Phys. Eng. Express* 2021, 7(6):065008.

[95] Kratochwil N, Gundacker S, Auffray E. A roadmap for sole Cherenkov radiators with SiPMs in TOF-PET. *Phys. Med. Biol.* 2021, 66(19):195001.

[96] Lee D, Cherry SR, Kwon SI. Colored reflectors to improve coincidence timing resolution of BGO-based time-of-flight PET detectors. *Phys. Med. Biol.* 2023, 68(18):185008.

[97] Haefner J, Neff A, Arthurs M, Batista E, Morton D, *et al.* Reflectance dependence of polytetrafluoroethylene on thickness for xenon scintillation light. *Nucl. Instrum. Methods Phys. Res. Sect. A* 2017, 856:86–91.

[98] Ghosh S, Haefner J, Martín-Albo J, Guenette R, Li X, *et al.* Dependence of polytetrafluoroethylene reflectance on thickness at visible and ultraviolet wavelengths in air. *J. Instrum.* 2020, 15(11):P11031.

[99] Loignon-Houle F, Pepin CM, Charlebois SA, Lecomte R. Reflectivity quenching of ESR multilayer polymer film reflector in optically bonded scintillator arrays. *Nucl. Instrum. Methods Phys. Res. Sect. A* 2017, 851:62–67.

[100] 3M Company. 3M™ Enhanced Specular Reflector Films (3M™ ESR). 2021. Available: https://www.3m.com/displayenhancement (accessed on 7 March 2026).

[101] Makek M, Bosnar D, Pavelić L. Scintillator pixel detectors for measurement of Compton scattering. *Condens. Matter* 2019, 4(1):24.

[102] Eljen Technology. Silicone Grease EJ-550, EJ-552. 2021. Available: https://www.eljentechnology.com/products/silicone-grease-ej-550-ej-552 (accessed on 7 March 2026).

[103] Romanchek G, Wang Y, Marupudi H, Abbaszadeh S. Performance of optical coupling materials in scintillation detectors post temperature exposure. *Sensors* 2020, 20(21):6092.

[104] Eljen Technology. Light guides and acrylic plastic. 2026. Available: https://www.eljentechnology.com/light-guides-and-acrylic-plastic (accessed on 7 March 2026).

[105] Bonesini M. Gamma-ray and high-energy X-ray detection with large-area scintillating crystals: a hands-on review. *Front. Detect. Sci. Technol.* 2025, 3:1551948.

[106] Wang B, Kreuger R, Beekman FJ, Goorden MC. Novel light-guide-PMT geometries to reduce dead edges of a scintillation camera. *Phys. Med.* 2018, 48:84–90.

[107] Jelinek M, Cip O, Lazar J, Mikel B. Design and characterisation of an optical fibre dosimeter based on silica optical fibre and scintillation crystal. *Sensors* 2022, 22(19):7312.

[108] Zhang H, Huang X, Wan T, Wei R, Yin B, *et al.* Integrated copper-halide activated scintillator fiber array for remote high-resolution X-ray imaging. *Nat. Commun.* 2025, 16(1):5973.

[109] Peterson TE, Furenlid LR. SPECT detectors: the Anger Camera and beyond. *Phys. Med. Biol.* 2011, 56(17):R145–R182.

[110] Radnia A, Alikhani A, Teimourian B, Nejad MY, Farahani MH, *et al.* Development of novel low-cost readout electronics for large field-of-view gamma camera detectors. *Phys. Med.* 2024, 121:103357.

[111] Deng Z, Deng Y, Chen G. Design and evaluation of LYSO/SiPM LIGHTENING PET detector with DTI sampling method. *Sensors* 2020, 20(20):5820.

[112] Cucarella N, Barrio J, Lamprou E, Valladares C, Benlloch JM, *et al.* Timing evaluation of a PET detector block based on semi-monolithic LYSO crystals. *Med. Phys.* 2021, 48(12):8010–8023.

[113] Winston R, Jiang L, Ricketts M. Nonimaging optics: a tutorial. *Adv. Opt. Photon.* 2018, 10(2):484–511.

[114] Kim C, Lee W, Melis A, Elmughrabi A, Lee K, *et al.* A review of inorganic scintillation crystals for extreme environments. *Crystals* 2021, 11(6):669.

[115] Hamamatsu Photonics K.K., Electron Tube Division. Photomultiplier Tubes: Basics and Applications, 4th ed. 2017. Cat. No. TOTH9001E04. Available: https://www.hamamatsu.com/content/dam/hamamatsu-photonics/sites/documents/99_SALES_LIBRARY/etd/PMT_handbook_v4E.pdf (accessed on 7 March 2026).

[116] Ghassemi A, Sato K, Kobayashi K. Technical guide to silicon photomultipliers (MPPC). 2022. Cat. No. KAPD9005E04. Available: https://www.hamamatsu.com/content/dam/hamamatsu-photonics/sites/documents/99_SALES_LIBRARY/ssd/mppc_kapd9005e.pdf (accessed on 7 March 2026).

[117] Scafè R, Pani R, Pellegrini R, Bennati P, Cinti MN, *et al.* Spectral matching factors for LaBr3: Ce crystals coupled to Hamamatsu H8500 family PMTs. *Nucl. Instrum. Methods Phys. Res. Sect. A* 2011, 643(1):89–94.

[118] Lavelle CM, Shanks W, Chiang C, Nichols M, Osborne J, *et al.* Approaches for single channel large area silicon photomultiplier array readout. *AIP Adv.* 2019, 9(3).

[119] Hamamatsu Photonics K.K. Photomultiplier Tubes and Related Products. 2020. Cat. No. TPMZ0002E02. Available: https://www.hamamatsu.com/us/en/product/optical-sensors/pmt/related-documents.html (accessed on 7 March 2026).

[120] Luan NT, Kim HJ, Lee HS, Truc LT, Jegal J, *et al.* Absolute light yield measurement of NaI: Tl crystals for dark matter search. *J. Instrum.* 2025, 20(6):P06024.

[121] Giaz A, Pellegri L, Riboldi S, Camera F, Blasi N, *et al.* Characterization of large volume 3.5 "×8" LaBr3: Ce detectors. *Nucl. Instrum. Methods Phys. Res. Sect. A* 2013, 729:910–921.

[122] Yu Y, Lv H, Tariq K, Liu D, Sheng X, *et al.* Study of the performance of photomultiplier tubes at high variable counting rates. *Nucl. Instrum. Methods Phys. Res. Sect. A* 2021, 1008:165433.

[123] Clampin M, Paresce F. Photon-counting imaging with a GaAs photocathode-evaluation of the Red-Ranicon for astronomical imaging. *Astron. Astrophys.* 1989, 225(2):578–584.

[124] Jinno T, Mori T, Ohshima T, Arita Y, Inami K, *et al.* Lifetime-extended MCP-PMT. *Nucl. Instrum. Methods Phys. Res. Sect. A* 2011, 629(1):111–117.

[125] Gys T. Micro-channel plates and vacuum detectors. *Nucl. Instrum. Methods Phys. Res. Sect. A* 2015, 787:254–260.

[126] Kosev K, Butterling M, Anwand W, Cowan T, Hartmann A, *et al.* Evaluation of a microchannel-plate PMT as a potential timing detector suitable for positron lifetime measurements. *Nucl. Instrum. Methods Phys. Res. Sect. A* 2010, 624(3):641–645.

[127] Semiconductor Components Industries, LLC. Introduction to the Silicon Photomultiplier (SiPM). 2023. Available: https://www.onsemi.com/pub/collateral/and9770-d.pdf (accessed on 7 March 2026).

[128] Semiconductor Components Industries, LLC. Silicon Photomultiplier (SiPM) High Fill-Factor Arrays. 2021. Available: https://www.onsemi.com/pdf/datasheet/arrayj-series-d.pdf (accessed on 7 March 2026).

[129] Gundacker S, Heering A. The silicon photomultiplier: fundamentals and applications of a modern solid-state photon detector. *Phys. Med. Biol.* 2020, 65(17):17TR01.

[130] Failla CR, Amaducci S, Poma GE, Finocchiaro P. Light readout of small scintillators using SiPM photosensors. *Sensors* 2025, 25(20):6412.

[131] Brinkmann L, Garutti E, Martens S, Schwandt J. Correcting the non-linear response of silicon photomultipliers. *Sensors* 2024, 24(5):1671.

[132] Moya-Zamanillo V, Rosado J. Understanding the nonlinear response of SiPMs. *Sensors* 2024, 24(8):2648.

[133] Otte AN, Garcia D, Nguyen T, Purushotham D. Characterization of three high efficiency and blue sensitive silicon photomultipliers. *Nucl. Instrum. Methods Phys. Res. Sect. A* 2017, 846:106–125.

[134] Dorosz P, Baszczyk M, Glab S, Kucewicz W, Mik L, *et al.* Silicon photomultiplier's gain stabilization by bias correction for compensation of the temperature fluctuations. *Nucl. Instrum. Methods Phys. Res. Sect. A* 2013, 718:202–204.

[135] Di Vita D, Buonanno L, Canclini F, Ticchi G, Camera F, *et al.* A 144-SiPM 3" LaBr3 readout module for PMTs replacement in gamma spectroscopy. *Nucl. Instrum. Methods Phys. Res. Sect. A* 2022, 1040:167179.

[136] Sarrut D, Bała M, Bardiès M, Bert J, Chauvin M, *et al.* Advanced Monte Carlo simulations of emission tomography imaging systems with GATE. *Phys. Med. Biol.* 2021, 66(10):10TR03.

[137] van der Laan DJ, Schaart DR, Maas MC, Beekman FJ, Bruyndonckx P, *et al.* Optical simulation of monolithic scintillator detectors using GATE/GEANT4. *Phys. Med. Biol.* 2010, 55(6):1659–1675.

[138] Decuyper M, Stockhoff M, Vandenberghe S, Van Holen R. Artificial neural networks for positioning of gamma interactions in monolithic PET detectors. *Phys. Med. Biol.* 2021, 66(7):075001.

[139] Carra P, Bisogni MG, Ciarrocchi E, Morrocchi M, Sportelli G, *et al.* A neural network-based algorithm for simultaneous event positioning and timestamping in monolithic scintillators. *Phys. Med. Biol.* 2022, 67(13):135001.

[140] Kinyanjui SM, Kuang Z, Liu Z, Ren N, Yang Y. Machine learning positioning algorithms for long semi-monolithic scintillator PET detectors. *Phys. Med. Biol.* 2025, 70(11):115018.

[141] Breitenmoser D, Cerutti F, Butterweck G, Kasprzak MM, Mayer S. Emulator-based Bayesian inference on non-proportional scintillation models by compton-edge probing. *Nat. Commun.* 2023, 14(1):7790.

[142] Daniel G, Yahiaoui MB, Comtat C, Jan S, Kochebina O, *et al.* Deep learning reconstruction with uncertainty estimation for γ photon interaction in fast scintillator detectors. *Eng. Appl. Artif. Intell.* 2024, 131:107876.